PRINTABLE ZIRCONIA MEMBRANES FOR HIGH POWER DENSITY MICRO SOLID OXIDE FUEL CELLS

BY

GREG B EISENMANN

THESIS

Submitted in partial fulfillment of the requirements
for the degree of Master of Science in Mechanical Engineering
in the Graduate College of the
University of Illinois at Urbana-Champaign, 2012

Urbana, Illinois

Adviser:

Professor Placid M. Ferreira

Abstract

Fuel cells are an emerging technology because of their ability to achieve high energy efficiency and low emissions. Among the various types of fuel cells, solid oxide fuel cells (SOFCs) have emerged as one of the most promising types, because of their fuel flexibility and there efficiency. The problem with SOFCs, however is the fact that they typically operate at the very high temperature range of 600-1000°C. This greatly limits the types of materials which can be used to build up the fuel cell. Additionally, this high operating temperature results in SOFC having slow start up and cool down times.

Because they have energy densities greater than that of normal batteries, there is an interest in creating micro SOFCs which could be used in portable devices such as laptops and cellphones. In order for this to be feasible, however, the operating temperature would need to be reduced. This can be done by reducing the thickness of the functional electrolyte membrane. In light of this, work has been done on the creating of ultrathin electrolyte membranes for use in low temperature SOFCs. However, most of the work done focuses on the creation of the membrane itself, and little mention is made on how a functional fuel cell would look or how it would be assembled. Indeed most of the membranes created do not readily lend themselves to being put into a fuel cell stack.

It is believed that the transfer printing technology developed at the University of Illinois provides a solution to the problem of how to assemble μSOFCs. Transfer printing would allow the ultrathin membrane electrode assembly (MEA) to be fabricated separately, and then put into place in a fuel cell support structure. This is beneficial because it allows the complicated MEA, with its porous anode and cathode, and dense electrolyte layer, to be created independently of the fuel cell structure itself. This is much simpler than the steps which would be required to fabricate the MEA and fuel cell structure simultaneously. Additionally, transfer printing would allow the fuel cell interconnect structure to be very thin (50-100 μm), thereby allowing a very high vertical density of the stacked membranes. That is, by making both the membranes and the interconnects thinner, high density μSOFCs can be achieved.

Crackfree ultrathin (650 nm) Ni/YSZ membranes for use in μSOFCs have been successfully fabricated, and the steps taken to achieve this are presented in this thesis.

Furthermore, these ultrathin Ni/YSZ membranes have been transfer printed onto a PDMS receiving substrate without incurring cracking. Although work remains to making fully functional membranes, the fact that these membranes can be transfer printed without cracking opens many possibilities for the future of solid oxide fuel cells. In light of this successful demonstration of the ability to transfer print Ni/YSZ membranes, a high power density fuel cell design based on the concept of transfer printing has been developed, and is presented with in this work.

To my loving fiancé, Diana Wagenbach, for her unending support of me during the preparation of this thesis.

Acknowledgements

I would like to thank my adviser, Placid M. Ferreira, for his mentorship and research assistance over the past two years. I would also like to thank my research group for their help and advice in working out the various challenges I encountered in my research.

I would like to specifically thank Steve Elgan, who allowed me to work with him as an undergraduate, and whose advice and mentorship during this time helped me understand how to function in a research environment.

I would like to thank Kyle Jacobs whose mentorship was greatly appreciated, and whose research advice was invaluable. He often helped me think through the challenges I was facing and provided valuable feedback regarding how I should proceed.

I would also like to thank Numair Ahmed and Miki Takagi for helping me figure out how to accomplish the various microfabrication steps required by my research project. Numair's vast knowledge of transfer printing, and his assistance in this step of the project was very helpful to me.

I would like to thank my fiancé, Diana Wagenbach, whose encouragement and support of me gave me the motivation I needed to finish this work.

Most importantly, I would like to thank my Lord and Savior, Jesus Christ, because without His grace and strength I would be nothing.

Table of Contents

Chapter 1: Introduction

1.1 Purpose and Motivation

Fuel cells are an emerging technology and are promising because of their ability to achieve high energy efficiency and low emissions. Solid Oxide Fuel Cells (SOFCs) have emerged as one of the most promising types of fuel cells because of their because of their high efficiency and fuel flexibility. The problem, however, is that SOFCs generally operate at 600-1000°C. This limits the types of materials which can be used in the construction of the fuel cell, as most materials would be unable to survive such extreme conditions. This high operating temperature also greatly limits the ability of the fuel cell to quickly cycle between the on and off state, as the thermal inertia of the system causes it to take a nontrivial amount of time to heat up and cool down. [1]

Many people are working on microscale SOFCs as a solution to this problem, as they can be operated at much lower temperatures and have much less thermal inertia. MicroSOFCs (μSOFCs) are emerging as a solution to this problem because they can be operated at lower temperatures and have much less thermal inertia. μSOFCs are also promising because of their potential for use in mobile devices and computers, as they have high power density. Fuel cells can achieve a higher power output with a lighter weight than existing batteries. Much work has been done on the creation of μSOFCs, with the main focus being on the creation and optimization of the membrane electrode assembly (MEA) [1] [2].

The purpose of this thesis is to demonstrate the use of polydimethylsiloxane (PDMS) based transfer printing to build high power density μSOFCs. Transfer printing will allow the electrolyte membrane to be fabricated separately and then placed into the fuel cell. Such a design would eliminate the need to create the fuel cell membrane and fuel cell structure simultaneously. More importantly, transfer printing allows components which are far too thin to be manually manipulated to be easily put in place in a functional device. This allows very high density fuel cell stacks to be assembled from individually fabricated components.

1.2 Challenges with Fuel Cells

Although a promising technology, there are many challenges to overcome before fuel cells can be solution to the energy problem. The biggest challenge faced while in creating SOFCs is the fact that they typically run at very high temperatures (600-1000°C). This causes several problems, not the least of which is the fact that this high operating temperature greatly limits the type of materials which can be used to construct the fuel cell stack. Also, the high temperature change experienced during start up and cool down can cause thermal stresses in the cell which can lead to membrane degradation and even membrane failure. This also causes fuel cells to have long start up and cool down times due to the thermal inertia of the cell. Although this might be okay in an industrial setting, to be practical as a battery for smaller applications, fuel cells need to have a much quicker startup time and if possible, a lower operating temperature.

Another challenge with fuel cells lies in the functional membrane itself. The membrane will be described in more depth later, but in general it requires a dense electrolyte with a porous electrode on either side. The fabrication of the membrane electrode assembly (MEA) is quite difficult and much research has been done on this [3] [4] [5] [6]. As already mentioned, the high operating temperatures require that the components of the membrane have comparable thermal expansions, to prevent bowing and cracking of the membrane. Therefore, work is being done to develop MEA materials which are thermally compatible with each other, and which properly catalyst the fuel cell reactions to ensure high efficiency operation [1].

1.3 Micro Fuel Cells

In light of the above mentioned challenges, much effort is being made to reduce the operating temperature of fuel cells. The best way to do this is to make the fuel cell membrane smaller, as there is a direct relationship between the membrane thickness and the operating temperature of the cell, as discussed in more depth later. There has been a focus on ultrathin fuel cell electrolyte membranes which can operate in the 350-500°C range [4] [5]. In addition to the lower operating temperature, the fact that these cells are quite a bit smaller, typically on the $1cm^3$ scale greatly decreases the thermal inertia of the cell, reducing the startup and cool down time.

Micro fuel cells have their own problems, however, not the least of which is the question of how to assemble such a cell. Whereas large fuel cells are able to be assembled by hand, there is a need for an assembly technique for a micro fuel cell. Additionally, the fabrications methods (tape casting, screen printing) which can be used for macro scale fuel cell membranes cannot be used to create ultrathin (100's of nanometers) membranes. The solution to this problem is achieved through microfabrication processes such as sputtering, evaporation and atomic layer deposition. Indeed much work has been done on using these methods to create functional fuel cell membranes [2] [6]. However, not much mention has been made in literature as to how to use the created membranes to build a functional fuel cell.

Furthermore, many of the membranes research are based on depositing the membrane materials on the top of a silicon wafer, then using backside etching to expose the membrane, as shown in Figure 1. In addition to the poor surface utilization of the membrane, the thickness of the wafer greatly limits the vertical density of membranes if they were to be placed in an actual fuel cell stack.

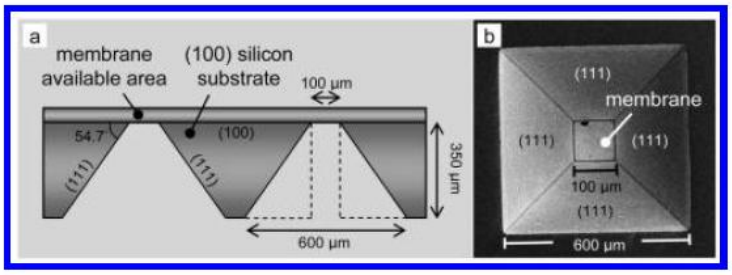

Figure 1. (a) Illustration of poor surface area utilization due to crystallographic constraints on KOH etching of (100) silicon substrate. (b) Membrane view from bottom. Four (111) planes confine the size of membrane. Percentage of surface utilization for 100 μm square membrane is only (100 μm)^2/(600 μm)^2 = 2.8%.

Figure 1 (a) Illustration of poor surface area utilization due to crystallographic constrains on KOH etching of (100) silicon substrate. (b) Membrane view from bottom. Four (111) planes confine the size of membrane. Percentage of surface utilization for 100 μm square membrane is only 2.8% [6]

1.4 Transfer printing as a fuel cell assembly method

It is believed that the transfer printing technology developed at the University of Illinois can offer a viable solution to the question of how to assemble a µSOFC. Heterogeneous transfer printing allows microscale components ("inks") to be picked up from a donor substrate and "printed" into place on a receiving substrate [7] [8] [9]. This assembly method (described in more detail later in this document) allows functional devices to be fabricated using standard microfabrication techniques, and then put into place in a larger system.

In the context of fuel cells, this means that fuel cell membranes can be independently created and then placed into a fuel cell structure. A fuel cell could then be built by stacking the various components together. This is similar in concept to a macroscale fuel cell stack, but would allow membranes on the order of 100's of nanometers thick to be put in place between 50-100µm spacers. A general concept of how this fuel cell stack would look is shown in Figure 2 and Figure 3.

This design allows for very high membrane surface density. More important, however, is the fact that the silicon spacers can be made to be very thin, thus allowing a high vertical density, as well. Said another way, transfer printing allows membranes to be very densely packed into place, thus allowing the fuel cell to have a greater volumetric power density.

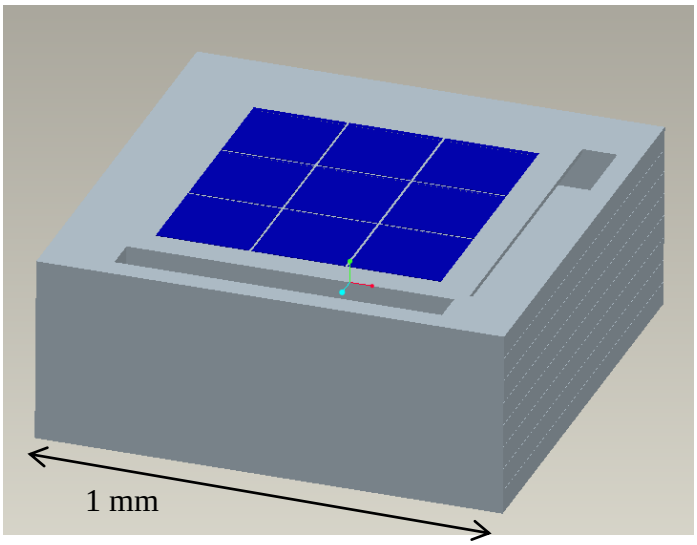

Figure 2 Fuel cell stack concept. Transfer printing would be used to place the MEA (blue) into a silicon interconnect structure.

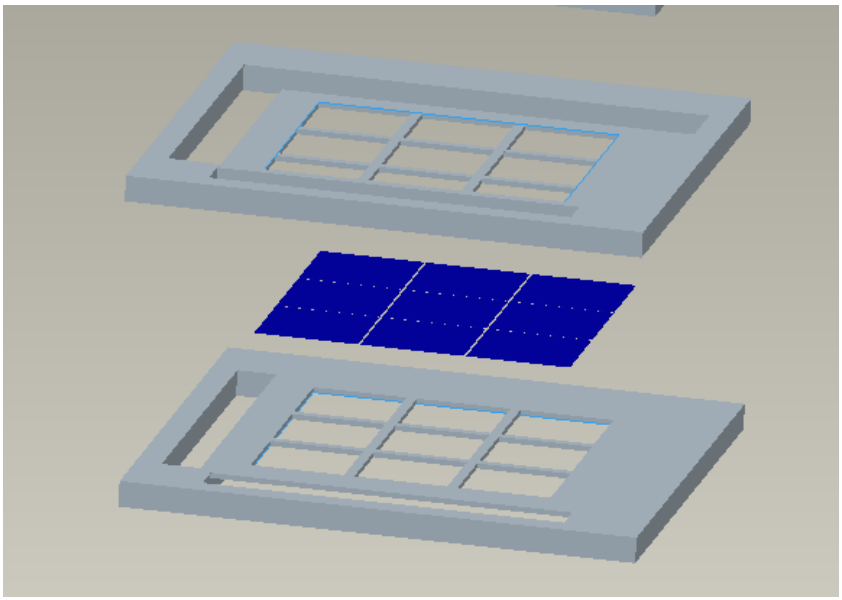

Figure 3 Fuel cell stack concept – exploded view. Blue- 650nm thick functional membrane. Grey – 50-100μm thick silicon interconnect structure.

1.5 Creation of Thin Membranes

Before transfer printing can take place, a suitable donor substrate containing fuel cell membranes must first be fabricated. The components of the membrane are required to be built up in such a way that they can then be lifted off of the surface of the substrate upon which they were created and transfer printed in place in the fuel cell stack. This can be achieved via standard microfabrication processing techniques, such as photolithography, etching, sputtering, etc.

1.6 Objectives and Scope of Thesis

Crack free, ultrathin Ni/YSZ (yttria stabilized zirconia) membranes have been fabricated using standard microfabrication methods. It has been demonstrated that these membranes can be transfer printed from a donor substrate to a receiving substrate without causing cracking or trauma to the membranes. In light of this demonstration of the feasibility of membranes to be transfer printed, a general concept for a transfer printed microfuel cell has been developed.

The specific objectives of this thesis are as follows:

- Explain the fabrication method used to create an array of transfer printable ultrathin zirconica membranes
- Demonstrate the ability to transfer print ultrathin YSZ electrolyte membranes onto a PDMS substrate
- Demonstrate the ability to transfer print crack-free ultrathin Ni/YSZ electrode-electrolyte membranes onto a PDMS substrate
- Demonstrate the ability to transfer print crack-free ultrathin Ni/YSZ electrode-electrolyte membranes onto a silicon frame
- Present a general design concept of how a μSOFC created via transfer printing would look.
- Demonstrate the theoretical feasibility of the design presented.

Chapter 2: SOFC overview

2.1 Introduction

Much work is being done to fabricate micro solid oxide fuel cells (μSOFCs). There are a wide variety of design concepts being worked on, including button cells ([10] [11] [12] [13]), tubular fuel cells ([14] [15] [16] [17] [18]), and ultrathin membrane fuel cells ([4] [5] [6]). Most of the work done is focused on the creation of the membrane electrode assembly (MEA), though some labs are focusing on the overall fuel cell design ([3] [19]). A thorough discussion of the work done on fuel cells and the current state of the art can be found elsewhere in literature [2].

Although different in geometry, all of the fuel cell works on the same basic principles. The purpose of this section is to give a general overview on the operation of a μSOFC.

2.2 Fuel cell overview

The basic premise of a fuel cell is to convert the stored chemical energy in a hydrocarbon fuel directly into electrical energy via the reactions at the anode and cathode. This is more efficient than a combustion engine because this conversion energy is not limited by the Carnot efficiency. Another benefit of SOFCs lies in the fact that a wide variety of fuels can be used, from pure hydrogen to natural gas and heavier hydrocarbons. The anode and cathode reactions are summarized below, and a general schematic of fuel cell operation is shown in Figure 4. Note that if pure hydrogen is used, the only byproducts are water and heat. This potential for clean energy is part of what makes fuel cells such a promising technology.

Anode: $H_2 + O^{2-} \rightarrow H_2O + 2e^-$

$CO + O^{2-} \rightarrow CO_2 + 2\ e^-$

Cathode: $O_2 + 4\ e^- \rightarrow 2\ O^{2-}$

Overall: $H_2 + CO + O_2 \rightarrow H_2O + CO_2 + \Delta E$

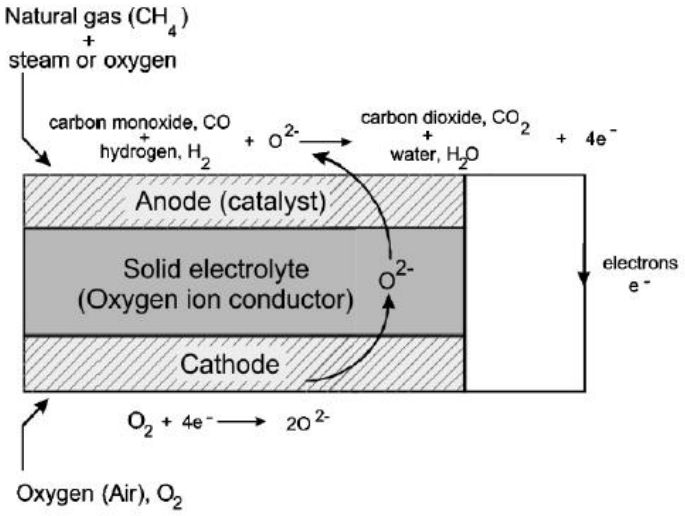

Figure 4 General schematic of SOFC operation [1]

2.2.1 Electrolyte

The purpose of the electrolyte is to provide a physical barrier between the oxygen and fuel, but allow oxygen ions to pass through to complete the electrical circuit. Therefore, the electrolyte must be dense and electrically insulated, but able to conduct ions. The electrolyte must also be stable in both and oxidizing and reducing atmosphere. The most commonly used electrolyte materials is yttria stabilized zirconia, though much research is being done to discover other materials with an even higher oxygen ion conductivity. This also relates to the fact that YSZ must be heated to high temperatures, usually on the order of 600-1000°C for the oxygen ion conductivity to be sufficiently high for fuel cell operation (the operating temperatures of fuel cells will be discussed in more depth later in this chapter).

Pure ZrO_2 is monoclinic at room temperature and undergoes phase transitions to a tetragonal structure above 1170°C and to the cubic structure above 2370°C. Yttria has a high solubility in ZrO_2 and stabilized the zirconia in the cubic fluorite structure. The addition of yttria also increases the concentration of the oxygen ion vacancies, which significantly increases the ionic conductivity of the zirconia. While other dopants can yield even higher ionic conductivities, they are also more expensive, so yttria is commonly used. It has been determined

that 8 mol % Y_2O_3 in ZrO_2 provides the highest ionic conductivity, so this is the most composition used in the electrolyte membranes [1].

2.2.2 Anode

The purpose of the anode is to catalyze the reaction on the fuel side of the membrane. The anode must be porous to allow fuel to flow through it, though must also be electrically conductive, as it acts as one of the electrodes for the fuel cell. Furthermore, the anode must be chemically stable in a reducing environment and must be able to survive the fuel cell operating temperatures, which are often in the 600-1000°C range. This limits the choice of anode materials to nickel, cobalt and noble metals. The most common choice of material for the anode is Ni, because it is relatively inexpensive compared to the other options.

The nickel is also required to have a similar coefficient of thermal expansion as the electrolyte membrane, as if it did not, severe cracking or delamination would occur during the thermal cycling experienced in normal fuel cell operation. To account for this, the nickel is often mixed with the solid electrolyte material to form a cermet. This cermet also helps to maintain the porosity of the nickel and prevent sintering during operation. However, the nickel content must be high enough to maintain the conductivity of the anode. The threshold for this is around 30 vol% Ni [1].

2.2.3 Cathode

The purpose of the cathode is to catalyze the reactions on the oxygen side of the membrane. The cathode must be porous to allow fuel to flow through it, though must also be electrically conductive, as it acts as one of the electrodes for the fuel cell. The cathode must also be chemically stable in an oxidizing atmosphere, even at high temperatures. Similar to the anode, the cathode must have a similar thermal expansion to the electrolyte, and must also not react with the electrolyte. One way to accomplish this is to mix in part of the electrolyte material with the cathode, though again care must be taken to maintain electrical conductivity.

Because noble metals are precluded for economic reasons, the cathode is often made out of electronically conducting oxides. Numerous doped oxides have been studied, with strontium-doped lanthanum manganite, $La_{1-x}Sr_xMnO_3$ (LSM) is the most commonly used. Another commonly used material is $La_{1-x}Sr_xCo_{1-y}Fe_yO_3$ (LSCF), though this material is problematic because of its reactivity with the YSZ electrolyte [1].

2.3 Fuel cell operating temperature

SOFCs typically operate at high temperatures, on the order of 600-1000°C, which is problematic because it greatly limits the choice of materials which can be used to construct the fuel cell. One method for reducing the fuel cell operating temperature is to make the electrolyte membrane thinner, as thinner membranes have a higher ionic conductivity at a given temperature. The ionic conductivity of YSZ is shown in Figure 5. According to theory (discussed elsewhere in literature) the area specific resistance, R" must be less than $0.2\Omega cm^2$ for sufficient fuel cell operation [4]. R" is related to the ionic conductivity, σ, and the membrane thickness, t, according to equation 1 below:

$$R * A = R'' = \frac{t}{\sigma} \quad (1)$$

Figure 6 shows the theoretical area specific resistance as a function of temperature for a number of different membrane thicknesses. It is readily apparent why high operating temperatures are required, as a 20um thick electrolyte membrane must be heated to above 700°C before the required minimum area specific resistance of $0.2\ \Omega cm^2$ is achieved. It is interesting to note, however, that much lower operating temperatures can be achieved with thinner membranes. Indeed it is the goal of many researchers, and is within the scope of this thesis, to produce an electrolyte membrane on the order of hundreds of nanometers thick for the very purpose of achieving low temperature fuel cell operation [4] [5].

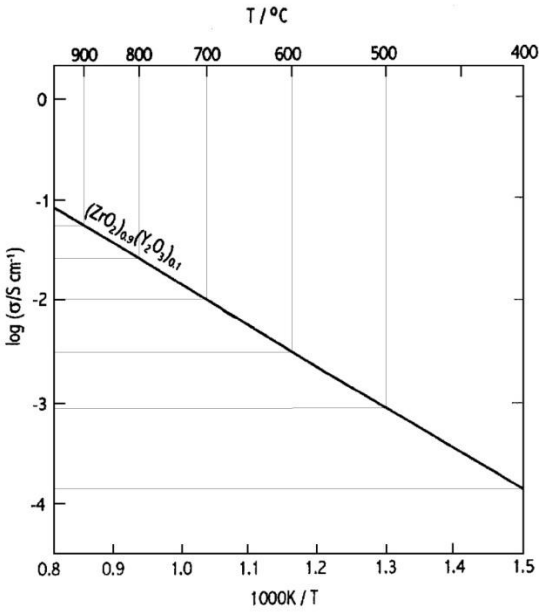

Figure 5 Ionic conductivity of YSZ

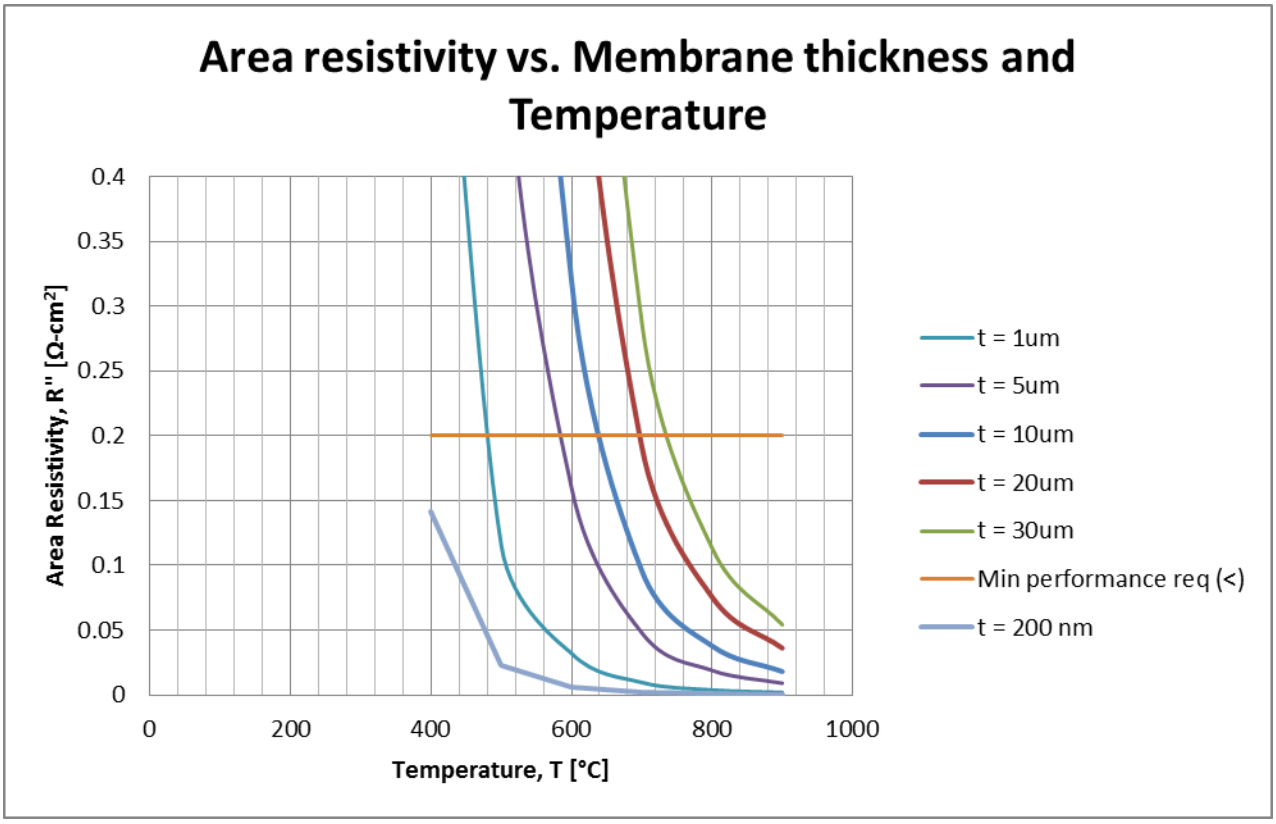

Figure 6 Theoretical area resistivity as a function of temperature for various membrane thicknesses

2.4 Problems faced

As mentioned, one of the biggest problems faced with SOFCs is the fact that the high operating temperature of 600-1000°C for traditional membranes highly restricts the type of materials which can be used for the construction of the fuel cell. In addition to material limitations, these high operating temperatures are also a problem because thermal inertia of the system leads to slow start up and shut down times. Furthermore, the greater the operating temperature, the more likely the membrane components are to rupture and delaminate from each other due to thermal expansion mismatches.

In light of these problems, there is much interest in creating fuel cells which have a lower operating temperature. As was seen in the previous section, this can be achieved by reducing the size of the electrolyte membrane. This, however, leads to more problems, as the electrolyte membranes become very fragile and must be supported. This is often achieved by using the anode to support the electrolyte, as the typical anode material, Ni, is quite inexpensive.

Additional problems with thin membranes pertain to the fact that as the membrane size decreases, it becomes far easier for defects or pinholes to cause the membrane to be gas permeable. Therefore, much care must be taken to ensure that the membranes are fully dense and crack free. Furthermore, methods of creating extremely thin films, such as sputtering or atomic layer deposition are more expensive and time consuming than the other commonly used methods, such as EPD, dipcoating, tape casting.

Another problem faced, as already alluded to, is material compatibility and adherence of the different membrane layers, especially in the presence of thermal cycling. This can be avoided by making multi-layered anodes and cathodes, with the layers closest to the electrolyte containing some of the electrolyte material, thereby softening the effect of the thermal expansion.

The fuel cell anode is also susceptible to poisoning, which is caused if sulfur is contained in the fuel. This reduces the active area of the anode and causes fuel cell performance to degrade. A full analysis of the problems faced in SOFCs is beyond the scope of this thesis, but is covered elsewhere in literature [1]

2.5 Fuel Cell performance

The fuel cell performance is often reported in terms of W/cm^2, though this is a deceiving metric as it does not give a good picture of the volumetric power density of the cell, which is the more important characteristic. Sossina Haile at Caltech is working on a fuel cell with a novel circular design, and reports an energy output of $1010W/cm^2$ at a temperature of 600°C [20]. Fritz Prinz, at Stanford University is working on ultrathin fuel cell membranes and reports an energy output of $400mW/cm^2$, though at the much lower operating temperature of 400°C [4]. Toshio Suzuki at the AIST in Japan is working on micro tube fuel cells, and reports a power output of $480mW/cm^2$ at 550°C, with a bundle performance of $2W/cm^3$. A full literature review on the state of the art regarding fuel cell technology is beyond the scope of this thesis, but may be found elsewhere [2].

In general, the power output of a fuel cell is given as a function of the current density, and is in the shape of a downward facing parabola, as shown in Figure 7 below. Therefore, any given fuel cell membrane will have a maximum power output at a given current density, dependent on the characteristics of the membrane. The voltage of a fuel cell can be calculated according to equation 2 below,

$$V = emf - J\,x\,ASR_e - \eta_{act} = emf - Jx\,ASR_e - \frac{RT}{\alpha nF} ln \frac{J}{J_o} \qquad (2)$$

where emf is the theoretical electromotive force, J is the current density, ASR_e is the area specific resistance of the electrolyte, R is the gas constant, F is the Faraday constant, J_o is the exchange current density and α is the corresponding transfer coefficient [4].

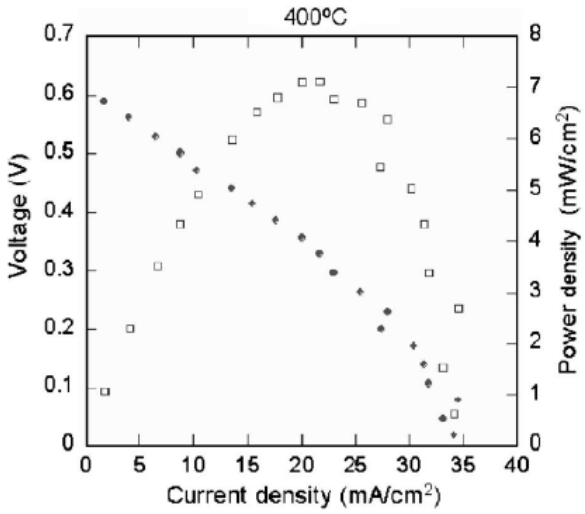

Figure 7 Characteristic fuel cell power/voltage output graph

2.6 Conclusions

Fuel cells are a promising technology because of their potential for high power density. This stems from the fact that high energy density fuels can be used, and that the chemical energy is converted directly into electrical energy, thereby avoiding Carnot limitations, due to the reactions at the cathode and anode. Due to the restrictive nature of the high temperature operation of normal fuel cells, much effort is being made to create fuel cells which can operate at lower temperatures. Additionally, the power output of a fuel cell is highly dependent on the membrane itself, so work is being done to optimize these characteristics. An in depth discussion of the mechanics of fuel cells is beyond the scope of this thesis, but may be found elsewhere [1] [2].

Chapter 3: Fuel Cell Design

3.1 Introduction

The premise of this work is to assemble a fuel cell with a high power density with the aid of transfer printing. Most papers report the fuel cell power outputs with regard to power output per unit area. This, however, does not speak to the volumetric output, and indeed, many of the fabricated membranes reported in literature would exhibit low volumetric power output because each component in the fuel cell stack would be so thick ([2] [4]).

Transfer printing (described in more detail later in this work) would greatly alleviate this problem because a fuel cell membrane could be independently created, and then put into place within a micromachined silicon interconnect structure. Because the membranes are only on the order of 500nm thick and because the silicon interconnects could be made to be on the order of 50um thick, this allow for very high stacking efficiency. The purpose of this chapter is to set for a general concept for how a high power density fuel cell could be realized with the aid of transfer printing.

3.2 General Stack Concept

The general concept behind the proposed fuel cell is to use the transfer printer to place the various components into a stack. The main components are a silicon spacer, with flow channels for the air and fuel, and with a structure into which the fuel cell membranes could be printed, and the fuel cell membranes themselves. The general stack concept is shown in Figure 8 and an exploded view showing the various components is shown in Figure 9. The Si structure would have holes configured such that the air would flow in series back and forth across each set of membranes, with fuel flowing in a perpendicular direction on alternating membranes. A side view of the fuel cell stack concept is shown in Figure 10, with the smallest repeatable unit, used for modeling purposes and defined to be a “block” being shown in Figure 11

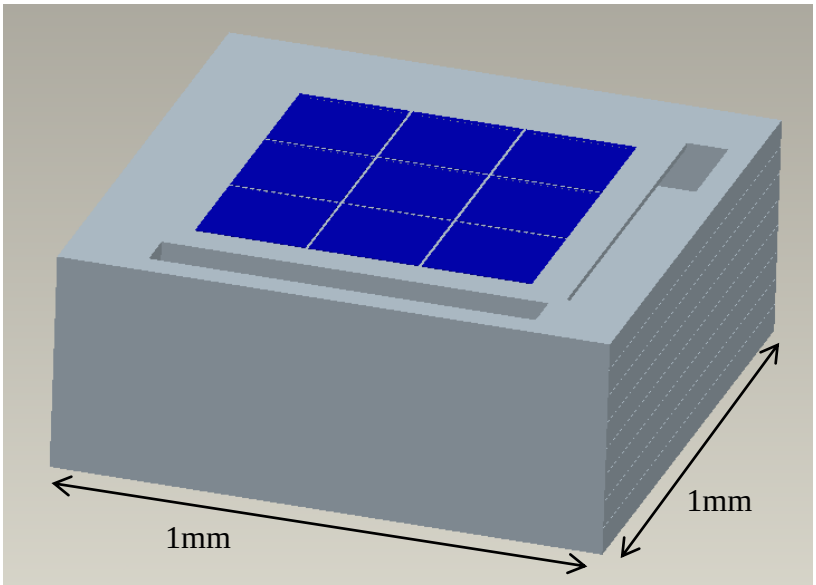

Figure 8 Fuel Cell Stack general concept

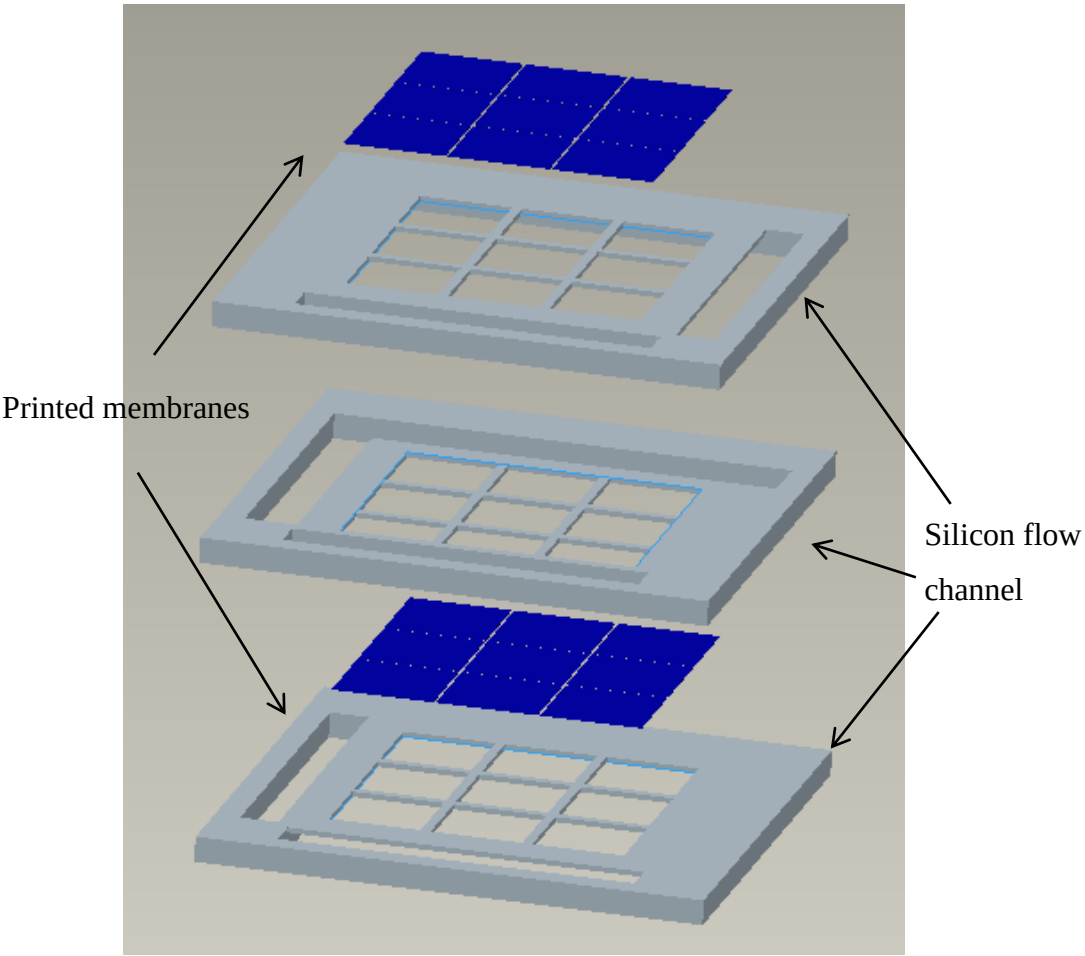

Figure 9 Exploded view showing stack components

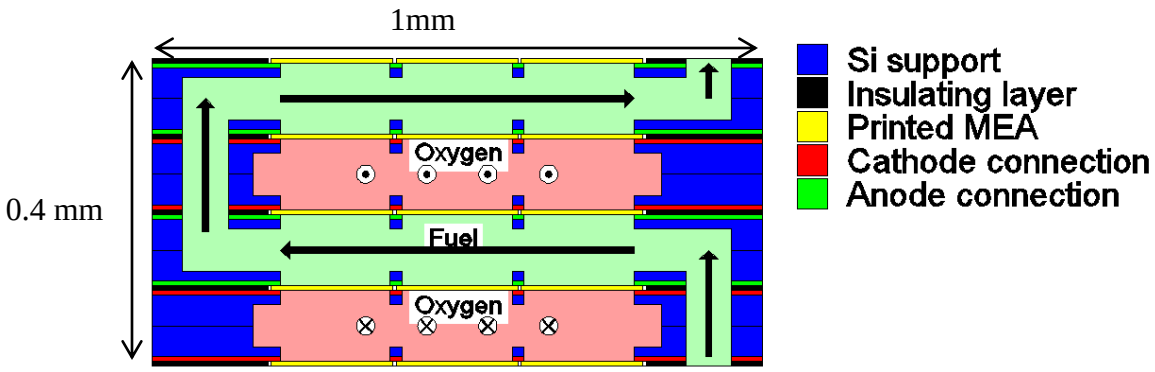

Figure 10 Side view of fuel cell concept.

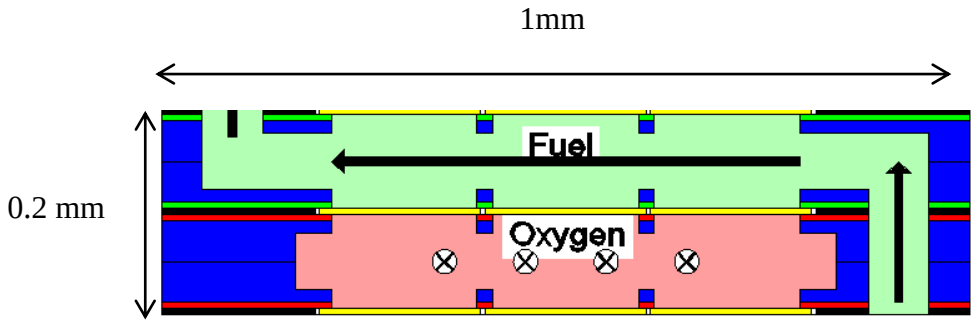

Figure 11 A "block", as defined for modeling purposes

3.3 Thermal analysis

As was mentioned in previously, fuel cell operation temperature is directly dependent on the membrane thickness and the desired area specific resistance. According to literature, the area specific resistance should be less than $0.2\Omega cm^2$ for the fuel cell to operate [4]. This, however, is simply a baseline, and the lower this value, the better the fuel cell performance. Based on Figure 6 above, and the fact that the fabricated fuel cell membranes are on the order of 350nm thick, it is expected that this fuel cell would operate at around 500°C.

For the fuel cell to be thermally sustainable, the heat lost must be less than the heat generated. The overall chemical balance of the fuel cell is expressed in equation 3 below. It is assumed that there is approximately twice as much N_2 as O_2 in air.

$$2H_{2\,@\,25C} + O_{2\,@\,25C} + 2N_{2\,@\,25C} \rightarrow 2H_2O_{@\,500C} + 2N_{2\,@\,500C} + \Delta H_c^\circ \quad (3)$$

For the fuel cell to be sustainable, the amount of energy lost in the exhaust gases must be less than the amount of energy generated by the formation of H_2O in the fuel cell. It is assumed that the gases will be introduced to the system at room temperature (25°C) and will leave the system at 500°C.

It was reported in literature that 100sccm of H_2 was sufficient to cover a $20mm^2$ membrane [21]. This yields a value of 5 x 10^{-6} sccm /μm^2. It is assumed that there will be 18 200µm x 200µm membranes per block (Figure 11) of the fuel cell stack. Assuming some area loss at the edge of the membrane, it is estimated that each block of the fuel cell will have an active anode area of 325,000μm^2. This suggests a required fuel flow of 3.25sccm H_2 per block. Assuming 5 blocks per stack yields a required flow of 16.25sccm as shown in equation 4 below

$$\frac{5\,x\,10^{-6}\,mL}{min{\cdot}\mu m^2} * \frac{325{,}000\mu m^2}{block} * \frac{5\,blocks}{stack} = 16.25\frac{mL}{min} = 16.25sccm\ H_2 \quad (4)$$

If 1 minute of fuel cell operation is assumed, this means that 7.3 x 10^{-4} mol H_2 will be consumed, according to equation 5 below:

$$\frac{16.25mL}{min} * \frac{8.988x10^{-5}}{mL} * \frac{mol\ H_2}{2g} *\ 1\ min = 7.3x10^{-4}\ mol\ H_2 \quad (5)$$

Based on equation 3 the volume of H_2O vapor and N_2 exhausted from the fuel cell can be computed, as shown in equation 6 and 7 below.

$$7.3\ x\ 10^{-4}\ mol\ H_2\ * \frac{2\ mol\ H_2O}{2\ mol\ H_2}\ * \frac{18\ g\ H_2O}{1\ mol\ H_2O} = 0.0131g\ H_2O \quad (6)$$

$$7.3\ x\ 10^{-4}\ mol\ H_2\ * \frac{2\ mol\ N_2}{2\ mol\ H_2}\ * \frac{28\ g\ H_2O}{1\ mol\ N_2} = 0.0204g\ H_2O \quad (7)$$

The energy lost by the exhaust H_2O and N_2 is given by equations 8 and 9 below, where c_p is the specific heat of the gases, evaluated at 500°C and 1 atm:

$$Q_{H20} = c_p * \Delta T * m = \frac{2.1341J}{gC} * 475C *\ 0.0131g\ H_2O\ = 13.27\ J = Q_{H20} \quad (8)$$

$$Q_{N2} = c_p * \Delta T * m = \frac{1.04J}{gC} * 475C *\ 0.0204g\ H_2O\ = 10.07\ J = Q_{N2} \quad (9)$$

The total heat lost to exhaust gases in one minute of operation is then:

$$Q_{lost,exhaust} = Q_{H20} + Q_{N2} = 13.27J + 10.07J = 23.34J \quad 10$$

In order to calculate the heat lost to conduction, convection and radiation, a simple model was developed. A 1 mm x 1mm x 1mm Si cube was assumed to be at 500°C. A lumped mass model was used so that thermal conduction with in the cube could be neglected. This is equivalent to assuming that Bi<<0.1, and was confirmed to be the case after the calculations were performed. Heat was assumed to be lost via radiation and convection from the four side walls and the top surface. The heat lost to radiation was found to be 0.7127W and the heat lost to convection was calculated to be 0.1422W, for a total cube heat loss of 0.2135W. Therefore the amount of heat lost by the cube in one minute, assuming a constant heat loss, is shown in equation 11 below:

$$Q_{lost,Si\ cube} = \frac{0.2135J}{s} * \frac{60s}{min} * 1\ \text{min} = 12.81J \quad (11)$$

The total amount of heat lost in 1 minute of fuel cell operation is then:

$$Q_{losl} = Q_{lost,exhaust} + Q_{lost,cube} = 23.34J + 12.81J = 36.15J \quad (12)$$

The amount of heat generated by the cell is based on the formation of H_2O from H_2 and O_2. The enthalpy of combustion, $H_c°$ of H_2 and the corresponding energy released in one minute of fuel cell operation is shown in equations 13 and 14 below:

$$\Delta H_c° = -286\frac{kJ}{mol} \quad (13)$$

$$Q_{generated} = \frac{-286kJ}{mol\ H_2} * \frac{1000J}{1\ kJ} * 7.3\ x\ 10^{-4} H_2 = -208.78J \quad (14)$$

The total amount of heat is then, where a negative number indicates a net heat gain:

$$Q_{overall} = Q_{generated} + Q_{lost} = -208.78J + 36.15J = -172.63J \quad (15)$$

According to equation 15, in 1 minute of operation, the fuel cell will have an energy increase of 172.63 J. This indicates that the fuel cell is thermally sustainable. However, it is noted that much effort is taken elsewhere in literature to recoup the heat lost to exhaust gases in

order to make the fuel cell sustainable, suggesting that perhaps some important factor has been overlooked by this cursory analysis. If this was indeed the case then a method for recouping the heat from the exhaust vapor may need to be introduced to the fuel cell design.

3.4 Flow Rate Analysis

Given the small ($1mm^3$) scale of the proposed fuel cell, it is important to determine if the flow pressured required to pump the gasses through the micro-channels in the fuel cell would be unreasonably high, thereby rendering the design impractical.

Pressure drop in a channel can be calculated according to

$$Q = \frac{\pi {r_H}^4}{8\mu L}\Delta P \tag{16}$$

where Q [m^3/s] is the flow rate, r_H [m[is the hydraulic radius, μ [kg/m-s] is the dynamic viscosity, L [m] is the flow length and ΔP [Pa] is the pressure drop. The hydraulic radius is defined as:

$$r_H = \frac{1}{2}D_H = \frac{1}{2} * \frac{4A}{P} = \frac{1}{2} * \frac{4(tW)}{2(t+W)} = \frac{tW}{t+W} \tag{17}$$

where t [m] is the channel thickness and W [m] is the channel width.

For modeling purposes, the fuel cell was broken down to its smallest repeatable unit, as defined by the "block" shown in Figure 11 above. The pressure drop in one block was calculated, then multiplied by 5 (the assumed number of blocks in a complete cell) to yield the total pressure drop.

A block was assumed to have two distinct flow areas: the vertical channels (t =75μm, W= 700μm, L= 200μm) and the horizontal cavity (t = 80μm, W=700μm, L=900μm). The dimensions given are approximate given the conceptual designs shown in Figure 8, Figure 9 and Figure 11. The flow rate was assumed to be 16.25sccm, according to equation 4 in the previous section. The dynamic viscosity, μ of the three gases considered were μ_{air}=3.64e-5 kg/m-s, μ_{H2-} =1.62e-5 kg/m-s, μ_{CH4}=2.35e-5 kg/m-s.

According to equations 17 and 18 and the values given above, the pressure drop per block in the vertical channels and horizontal cavity (assuming the fluid is air) was 4.8Pa and 3.0Pa respectively, for a total pressure drop per block of 7.8Pa, or $1.1x\ 10^{-3}$ psi. Given the assumption of 5 blocks per fuel cell stack, a total pressure drop $5.6x10^{-3}$ psi is expected as the air travels through the fuel cell cavities. Based on similar calculations, the total pressure drop expected for $CH_4 = 3.6x10^{-3}$ psi and $H_2 = 2.5x10^{-3}$ psi.

Although far from an in depth analysis of the flow pressures, this cursory analysis is sufficient to show that the expected pressure drops in a $1mm^3$ fuel cell are minimal and are well within reason. This result makes sense in light of the fact that the required volumetric flow rates are quite small, and the flow cavities have been made to be relatively large in proportion to the fuel cell design. As long as the final fuel cell has a comparable design, in terms of flow rates and channel dimensions, it can be reasonably stated that the flow pressures will not become impractical.

3.5 Conclusions

A general design for a fuel cell created with transfer printing has been suggested. This fuel cell would have a high power density due to the ability to stack many cell layers very close to each other. A general flow analysis shows that the pressures encountered with such a design would be reasonable. Simple thermal analysis shows that the heat lost due to convection and radiation from the $1mm^3$ fuel cell would be minimal. Additionally, the heat lost to the exhaust gases was also shown to be insignificant. Therefore, the proposed design has been generally shown to be thermally sustainable and to be practical in terms of the required flow pressures.

Chapter 4: EPD of thin films

4.1 Introduction

One highly researched method for creating the electrolyte membranes for SOFCs is electrophoretic deposition (EPD) [11] [22] [23] [24]. EPD is a colloidal process in which particles are moved toward and then deposited on a charged electrode via the applied electric potential. This is a highly versatile process as it can be applied to many different geometries and requires inexpensive equipment [10]. Furthermore, the processing time is relatively short and the parameters of the deposited film, such as thickness, deposition rate and density can be controlled.

An attempt was made to use EPD to create crack free YSZ electrolyte membranes for use in solid oxide fuel cells. If successfully completed, these electrolyte membranes would have been transfer printed into place. Although many parameters such as thickness and grain structure were able to be successfully controlled, we were never able to achieve membranes which were completely crack free. The purpose of this section is to explain the steps taken towards crack free membranes and the lessons learned along the way.

4.2 Overview of EPD theory

EPD is a combination of electrophoresis and deposition. Electrophoresis is the motion of charged particles in a suspension under the influence of an electric field. Deposition is a coagulation of particles to a dense mass. In EPD, particles suspended in a colloid are subjected to an electric field. Because the particles are charges, this induces particle motion towards the oppositely charged electrode. Upon arrival to the electrode the particles deposit onto the surface. This exact theory of how and why this happens is quite complicated and is beyond the scope of this thesis, though has been covered extensively elsewhere in literature [10] [25]

Although the theory behind EPD is quite complicated, there is a nice equation relating multiple deposition parameters to the deposition weight, as shown by equation 18

$$w = \frac{2}{3}\frac{C\varepsilon_0\varepsilon_r\zeta Et}{\eta L} \tag{18}$$

where C represents the concentration of the suspension, ε_o the permittivity of free space, ε_r the relative permittivity of the solvent, ζ the zeta potential of the particle in the suspension, η the viscosity of the solvent, E the applied potential, L the distance between electrodes, and t is the deposition time [11]. The important thing to note about this equation is that for a given colloid with a given permittivity, zeta potential and solvent viscosity, the deposition weight, and by extension, thickness, can be directly controlled by controlling the colloid concentration, the applied voltage, the electrode separation and the deposition time. The relative ease with which these parameters can be controlled makes EPD a versatile, useful method of ceramic processing.

4.3 EPD setup

One of the most important aspects of electrophoretic deposition is the colloid itself. At its most basic level the colloid is a stable suspension of particles. If unstable, the particles will quickly settle to the bottom of the container, thereby rendering EPD impossible, or at least highly uncontrollable.

4.3.1 Colloid mixture

The following explains the steps taken to create the colloid for the EPD process. Note that this process was gradually modified during the course of the research that the process describes represents the final and most updated process used. An attempt will be made to explain the reason behind each choice in the colloid setup. A summary of the parameters used in the colloid preparation is given in Table 1

A standard solvent amount of 50mL was chosen as this was a good amount of liquid to work with. A mixture of acetone and ethanol was used, and an attempt was made to determine the proper ratio to get the maximum benefit out of both of these solvents. Acetone allows for faster deposition and yields a smoother film, but it has a very low surface tension, which causes the solvent to quickly evaporate from the sample upon removal from the solution [23]. This rapid evaporation causes large cracks to form on the surface of the deposition. Ethanol, which has a much higher surface tension, is therefore used to counter this rapid drying. However, ethanol also causes slower, rougher deposition, so cannot be exclusively used. A mixture of 60mL acetone and 40mL ethanol seemed to achieve the proper balance between deposition rate

and quality and cracking, and is what was ultimately used. This was very similar to the optimal ratio of 75mL acetone to 25mL ethanol set forth by a paper devoted to the discussion of acetone and ethanol based colloids [23].

Upon mixing the acetone and ethanol in a 4 oz glass container, the next step was to add iodine (207772, Sigma-Aldrich) for use as a surfactant. The iodine serves to increase the zeta potential of the colloid, which is directly related to the colloid stability. It was determined both experimentally and through literature survey that an I_2 concentration of 0.5g/l was sufficient to yield a stable colloid [24]. Additional I_2 beyond this concentration did not further increase the zeta potential, and even led to a decrease in the deposited mass of YSZ [24]. Based on this a standard amount of 25mg I_2 per 50mL solution (0.5g/l) was used.

The final component in the colloid is the YSZ (TZ-8Z, Tosoh) powder. Though other concentrations are used, the most common concentration seen in literature is 10g/L [23] [24]. This was experimentally confirmed as solutions with a low concentration yielded little or no deposit, and solutions with a high concentration of YSZ were unable to be made stable, with the YSZ immediately settling out of the solution, even after sonication. Given this, an amount of 0.5g YSZ per 50 mL solution was used.

The powder used had a given specific surface area of 16+-3m^2/g, which, along with a density of YSZ of around 5.9g/cm^3, yields a theoretical particle size of around 31.8nm. The actual particle size, as determined by visual inspection of the powder via SEM, was closer to 50nm, as shown in Figure 12. Regardless, this is far below the 1um size limit required to create a stable suspension specified in literature [10].

The final step in the preparation of the colloid was to ultrasonicate the mixture to create a stable suspension. If not done, the YSZ particles would quickly settle out of the solution, even after vigorous shaking. It was determined that placing the closed glass container with the colloid solution in an ultrasonic vibrator for 2.5 hours, with manual agitation every 10-15 minutes yielded a colloid which remained stable for at least 2 hours. It was observed that sonication caused the colloid to heat up and not properly stabilize, so ice was added to the sonication liquid to keep the temperate around 5-20°C. The exact temperature was not determined to be critical, as long as the colloid was prevented from heating up much beyond room temperature.

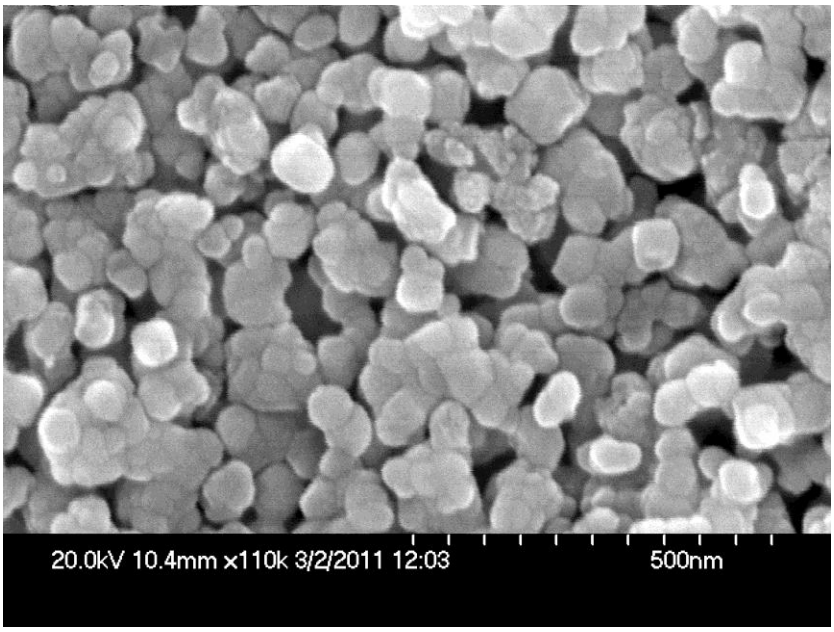

Figure 12 Unsintered YSZ particles (TZ-8Z) after electrophoretic deposition. Note particle size is around 50nm.

Table 1

Component/Step	**Amount**
Sovent	20mL Ethanol 30mL Acetone
Surfactant	25mg I_2 (0.5g/L)
Particles	0.5 g YSZ (10g/L)
Sonication time	2.5 hours
Temperature	5-20°C

4.3.2 EPD setup

The colloid created yields positively charged particles, so cathodic EPD was observed. This means that under the presence of an electric field, the YSZ particles would move toward and deposit on the cathode. It is important that the electric field be controlled, to prevent

unwanted deposition on the sample holder. In light of this a sample holder, shown in Figure 13 below was constructed out of Teflon. The holder was designed to allow two removable 5mm x 2.5mm plates to be held parallel to each other at a distance of 2.25cm. The anodic plate was a 2.5mm x 5mm x 0.8mm stainless steel plate. The cathodic plate was a similarly sized piece of Teflon upon which the samples could be mounted via conductive copper and carbon tape, as shown in Figure 14. This device was designed to be fit into a 100mL glass beaker and allowed alligator clips from a power supply to be attached at the top of the anode and cathode, but above the colloid itself, as shown in Figure 15. A general schematic of the concept of EPD is shown in Figure 16.

Figure 13 Teflon sample holder for EPD

Figure 14 Sample mounted to Teflon backing plate with carbon tape. Copper tape is used to ensure sample is negatively charged.

Figure 15 Teflon deposition cell with alligator clips attached to anode (SS plate) and cathode (Teflon plate with sample mounted to it)

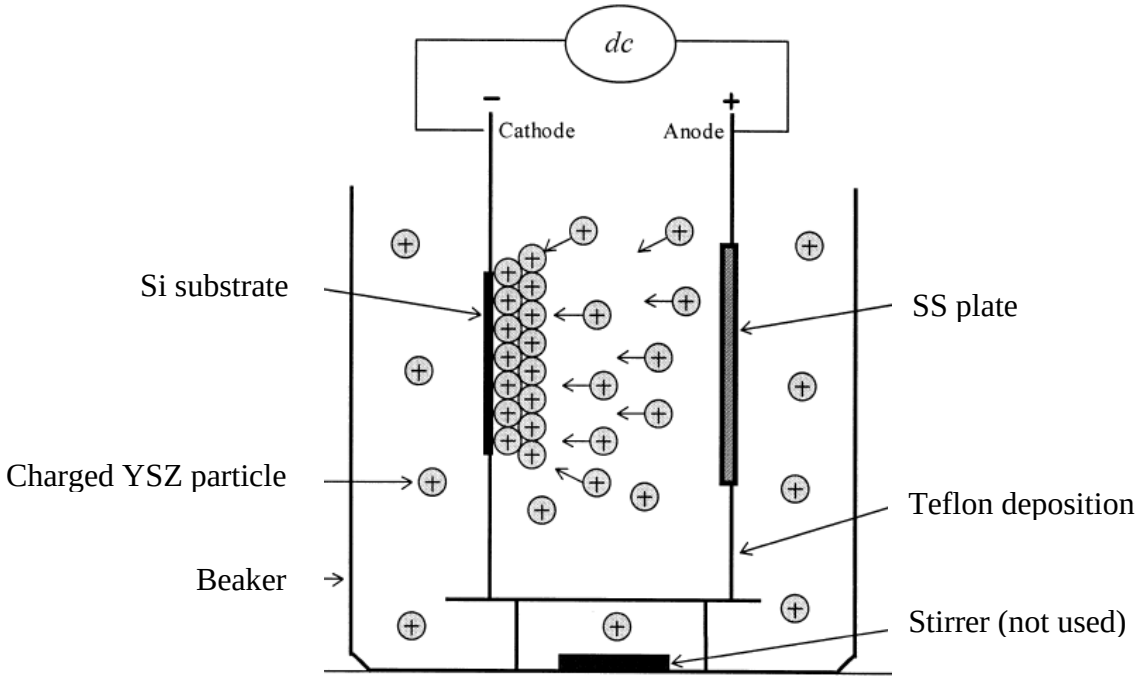

Figure 16 Schematic of cell configuration for EPD [24]

4.3.3 Sample preparation

The goal of this project was to use EPD to create crack free YSZ membranes for use in microsolid oxide fuel cells. According to literature, membranes on the order of 10-20 um thick could be produced in with deposition times from 5-10 minutes using electric fields from 10-40V/cm [10] [11] [12] [23] [24] [26]. Ultimately, the goal was to use the transfer printer developed at the University of Illinois to place the fuel cell membranes into a fuel cell structure. Traditional transfer printed membranes are around 100-250um square, so this was used as a starting point for the size of membranes produced. Therefore, an attempt was made to create an array of 230um x 230 um x 10 um membranes on a standard silicon die, using EPD.

In order to accomplish this, a 200nm thick layer of Ni was sputter coated onto Si dies using DC magnetron sputtering. This was done to create a conductive layer onto which the YSZ could be electrophoretically deposited. A 17 um thick SU-8 film was then spun on the Ni film. Standard photolithography techniques were used to pattern the SU-8 into a grid, as shown schematically in Figure 17 below. The purpose of the grid was to create a physical barrier to prevent YSZ from depositing on certain areas of the Ni during the EPD process.

The die with patterned SU-8 was then mounted to the Teflon sample holder, as shown in Figure 18. Copper tape was used to create the electrical connection between the alligator clip and the sample itself. However, copper tape did not maintain adhesion in the acetone-ethanol solution, so carbon tape was used to hold the sample in place. It was noted that deposition occurred on the copper tape, but not on the carbon tape. This suggests that the carbon tape was not sufficiently conductive to allow EPD to occur, and that therefore it did not cause distortion to the electric field.

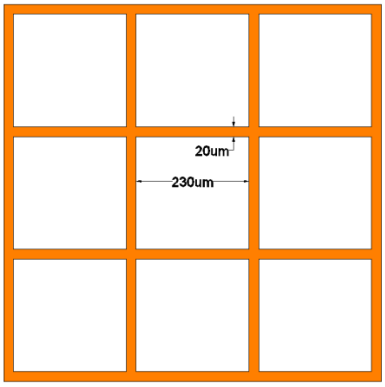

Figure 17 Schematic of SU-8 pattern used. Orange represents 17 um thick SU-8, white represents area into which YSZ will be deposited.

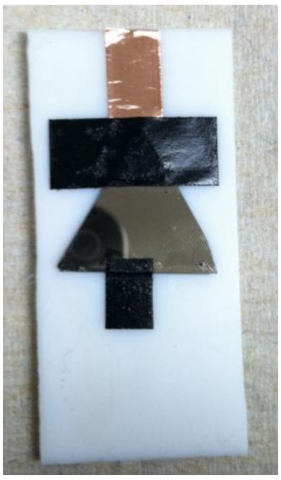

Figure 18 Si die patterned with SU-8 grid and mounted to Teflon sample holder

4.3.4 Deposition parameters

As mentioned in the theory section, the thickness of the deposited membrane can be readily controlled by changing the applied voltage and the time of the deposition. Higher voltage yields faster deposition. If the applied voltage is too high, however, the films will have a low density and be poorly formed [24]. If the applied voltage is too low then deposition will be extremely slow or nonexistent. Upon experimenting, it was determined that an applied voltage of 30V (yielding an electric field of 13.33V/cm, given the 2.25 cm spacing used), for 6 min yield

a deposition thickness of around 10um. Although an attempt was made to determine exactly what voltage yield the best films, in terms of density, grain growth and being crack free, this was never conclusively determined. This was because the membranes were never able to freely release from the substrate while being sintered, so as such exhibited dramatic variability in the resulting grain growth and density. Given this, the optimum value specified in literature of 13.33V/cm was used [24].

Another source of variability was the colloid itself. Though much effort was expended to create the colloid in a consistent manner, this was nearly impossible given the unpredictable manner in which the particles would settle out of the colloid with time. Though large particles would settle out fairly quickly, the smaller particles would slowly settle down to the bottom of the solution, thereby creating a gradient in the concentration across the colloid. Furthermore, with every deposition the amount of YSZ in the solution decreased, which also affected the deposition rate. This perhaps could have been alleviated with the introduction of a stirrer bar, though this also would have affected the motion of the charged particles in an unpredictable way.

Despite this unpredictability, 10um films were able to be reproducibly created. Generally speaking, the samples were mounted to the holder (as described above) and subjected to a 30V potential for 6 minutes. Upon completion of the deposition, the films were immediately placed into ethanol vapors to cause the drying to occur slowly and without introducing cracks into the film. (This was accomplished by putting a small amount of ethanol in the base of a beaker, and them placing the samples in the beaker.) It is believed that this allowed the solvent to evaporate out of the deposition slowly enough to prevent catastrophic cracking, due in part because of the fact that these films were relatively thin. Figure 19 below shows an SEM image of the film deposited by EPD, before it was sintered. Figure 19 shows no obvious cracks, but another image, shown in Figure 20 indicates that cracks can begin to form before sintering, though it is unknown whether this sample was subjugated to slow drying in ethanol.

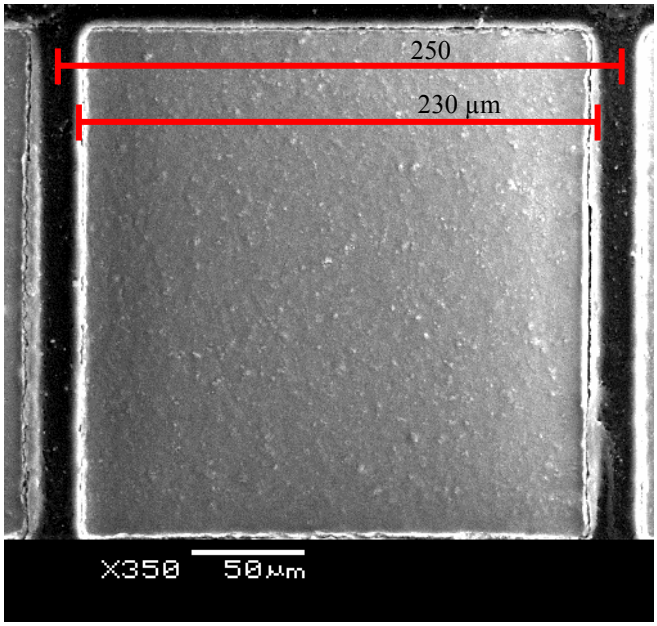

Figure 19 YSZ square after EPD, but before sintering. No obvious cracking

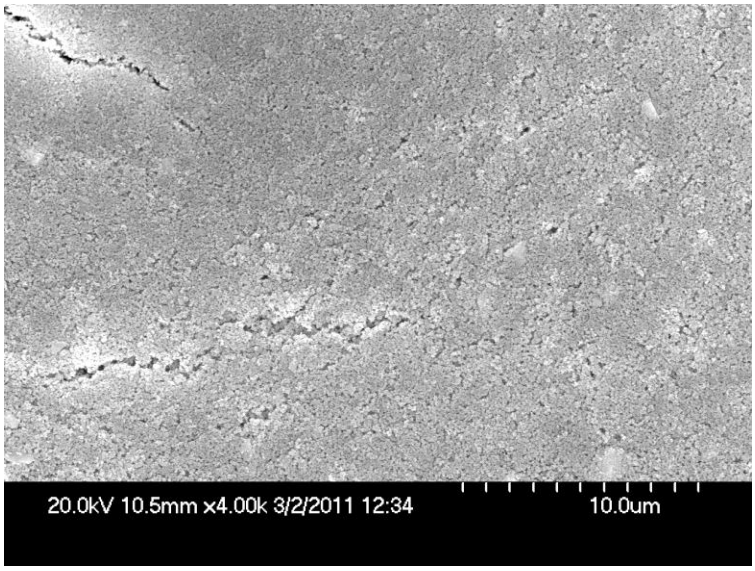

Figure 20 Unsintered YSZ particles after being electrophoretically deposited on Ni. Note formation of cracks

4.3.5 Sintering

Upon completion of the deposition, the samples were sintered at 1400°C for 2 hours with a ramp rate of 500°C/hr. This was concluded to be the optimal sintering temperature based on a

literature review, and was therefore consistently used [22]. Higher sintering temperatures would have yield even more grain growth, but were prevented by the fact the Nickel membrane had a melting point of 1457°C.

It is believed that the sintering step was ultimately the step that caused the membranes to crack. This is because upon sintering, the deposited green film of YSZ particles undergoes significant shrinkage and densification. However, the YSZ adhered strongly to the Ni, which caused the membranes to crack and to be highly porous, especially in the center of the membrane. Figure 21 shows that the YSZ shrunk more at the top of the deposition (230um to 199um, or 13.5%) than at the bottom (230um to 215um, or 6.5%). However, even the 13.5% shrinkage see at the top is far short of the 25-30% shrinkage expected. This indicates that the membrane is adhering to the Ni, which is preventing the YSZ from shrinking freely while being sintered. This can be further seen in Figure 22 which shows that grain growth could occur on the edges, where shrinkage was allowed, but that the sample remained porous in the center.

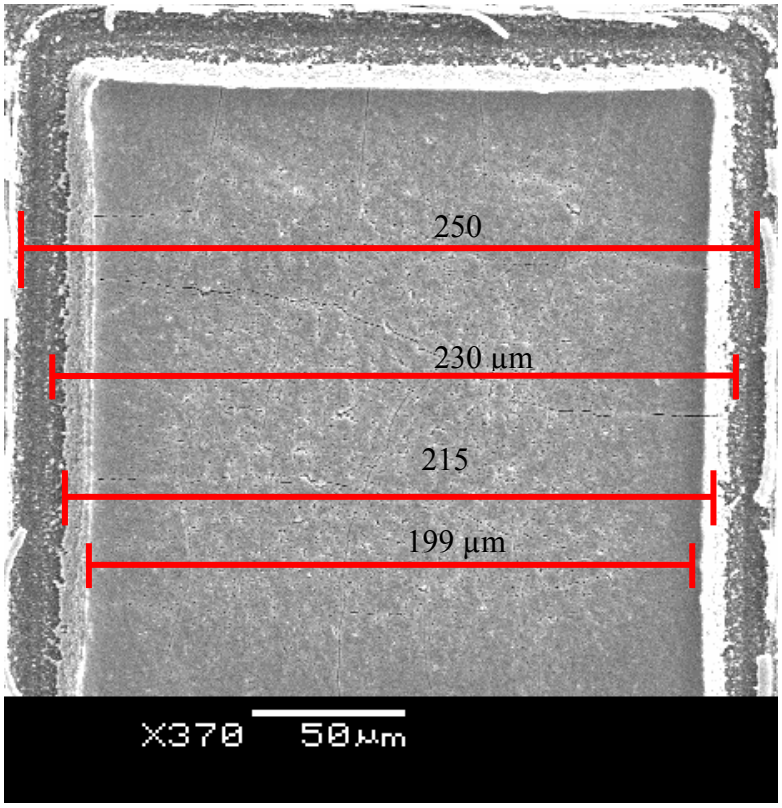

Figure 21 YSZ membrane after sintering. Note porosity and cracking due to inability of membrane to release from surface and completely shrink.

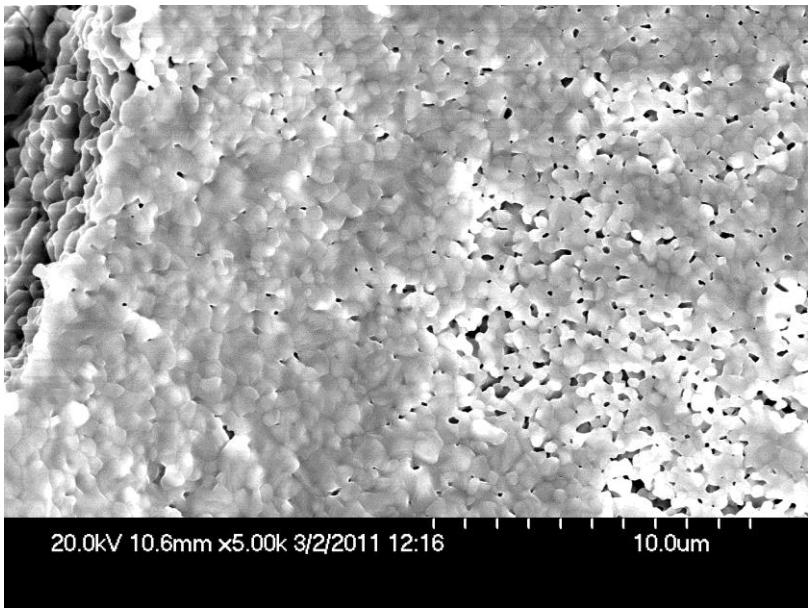

Figure 22 Dense grain growth and less porosity achieve on edge of square, because allowed YSZ film release

It was observed that the YSZ films deposited directly onto a Ni surface were strongly adherent to the Ni and therefore were prevented from shrinking freely when being sintered. It is believed that this prevented grain growth, and caused porosity and cracking in the films. Many steps were taken to allow free release of the membranes, but no successful method was determined. A brief summary of each method tried is prevented in this section.

4.3.6 Cr release layer

Some of the samples tested had a 120 nm sputtered Cr layer for the cathode in the EPD process. It was observed that several of the YSZ squares released from the Cr surface during the sintering step, and were allowed to shrink freely, thus causing no cracking and good grain growth, as shown in Figure 23 and Figure 24. It is unknown what caused these squares to release, however, as this result could not be repeated, and regardless had only occurred on 1-2 of the squares anyways. This result does indicate, however, that if the squares are allowed to freely shrink, they become quite dense and crack free. It is quite difficult, however, to cause this release to freely occur, as explored in the next sections of this chapter.

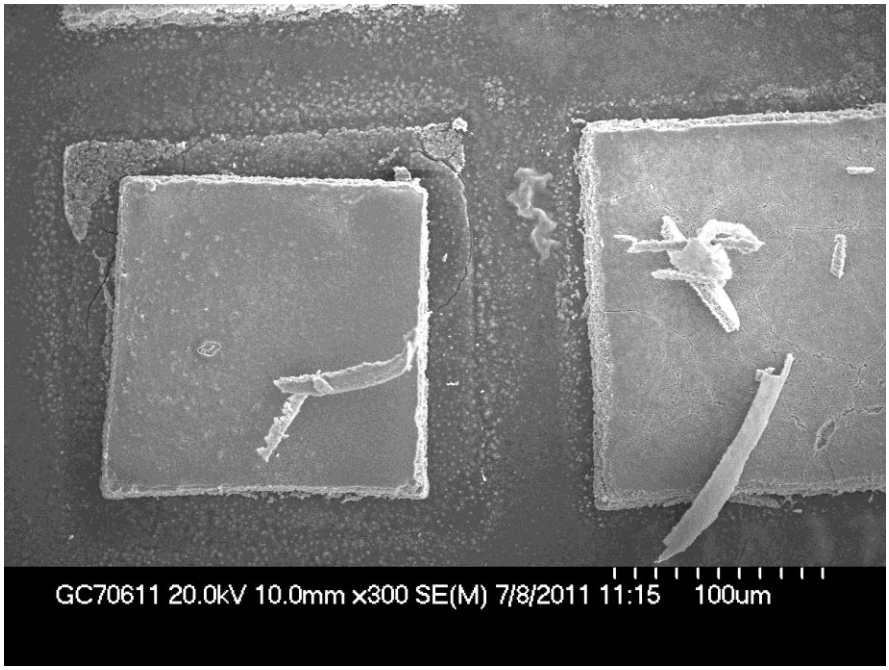

Figure 23 YSZ deposited via EPD on 120nm Cr layer, then sintered. One square, shown above, released from the Cr and was able to freely shrink and become dense without cracking.

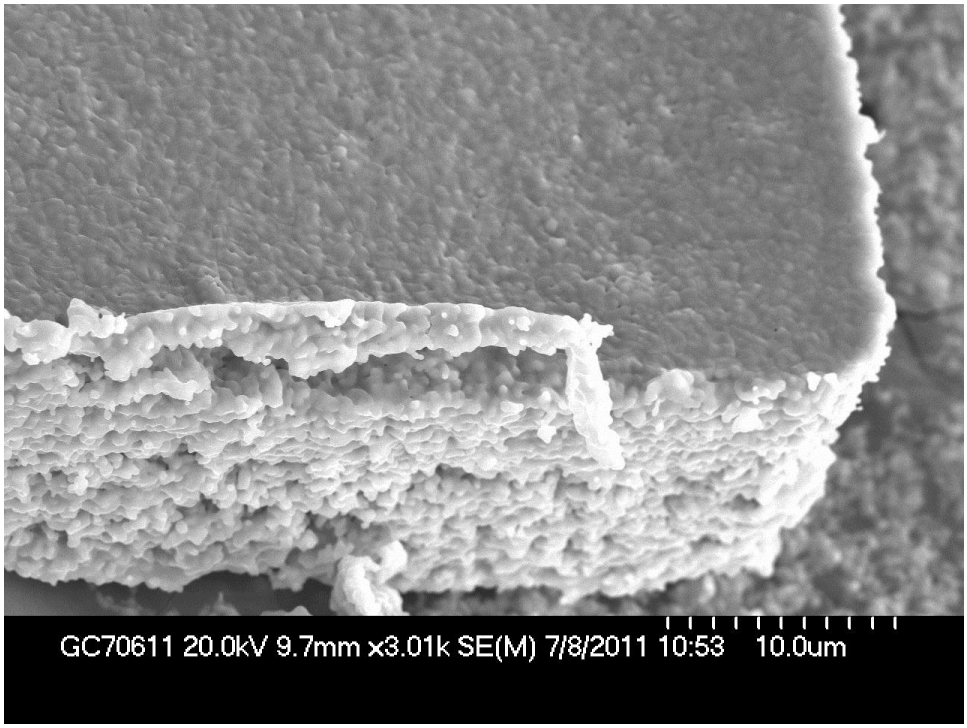

Figure 24 Large grain growth and densification possible if YSZ allowed to release from substrate and freely shrink.

4.3.7 Polymer Binder

One method of preventing cracks is to introduce a polymer binder into the colloid. This binder gets deposited along with the particles and serves to hold the particles together while drying. The binder then gets burned out during the sintering step [10]. Several polymer binders can be used, including poly(diallyldimethyalmmonium chloride) (PDDA) (409014, Aldrich) and polyvinyl butyral (PVB) (182567, Aldrich) [27] [28].

It was observed that addition of the PDDA binder caused catastrophic failure of the samples, as shown in Figure 25. The first problem observed was that the binder formed a stringy solution in the colloid. This string floated around in the colloid, but never dissolved or settled out. It is unknown what specifically caused this, but it did serve to cause very poor deposition, even initially. The cracking therefore may have come from the poor deposition, or the burnout of the polymer binder. Regardless, this lack of success did not seem promising and was not pursued further.

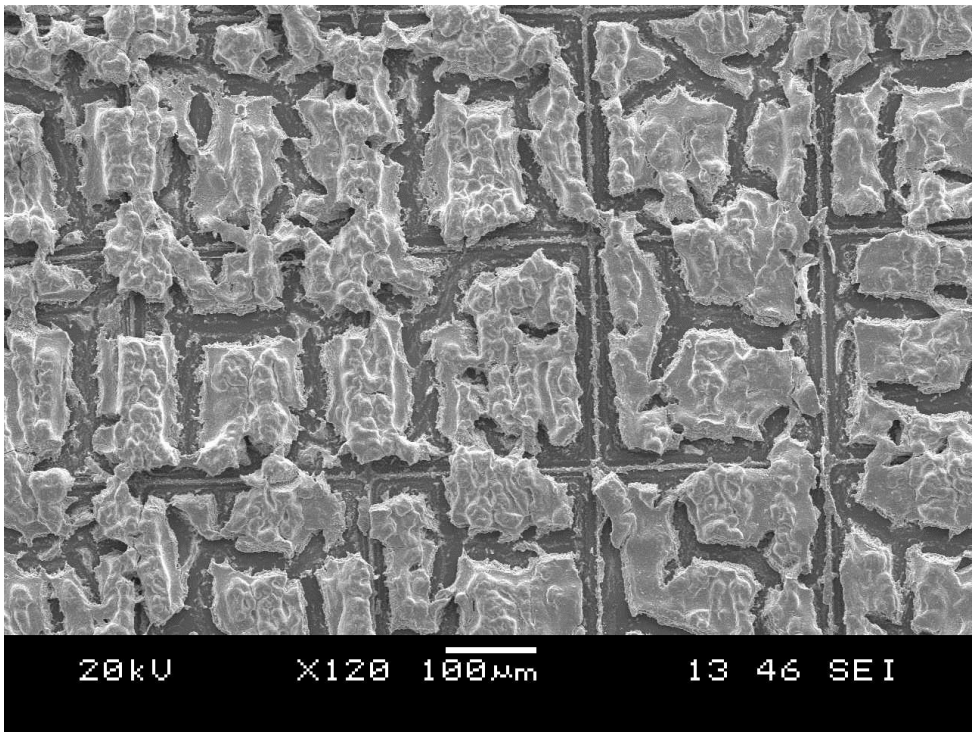

Figure 25 Catastrophic failure of membranes with addition of PDDA binder

The PVB performed slightly better, but still did not yield crack or defect free membranes. Upon sintering, at least one square seemed to release and become crack free (Figure 26). However, it appears that the burnout of the binder caused holes to be introduced to the surface of the deposit. These holes were consistent across the sample, much of which was not crack free anyways (Figure 27). These results led to the conclusion that PVA was not a good solution to create crack and defect free YSZ membranes

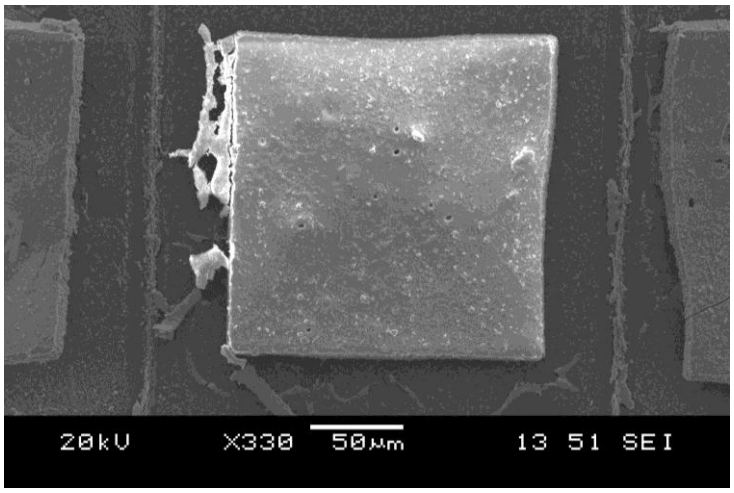

Figure 26 YSZ square after EPD with colloid with PVA binder and subsequent sintering. PVA burnout caused holes in sample.

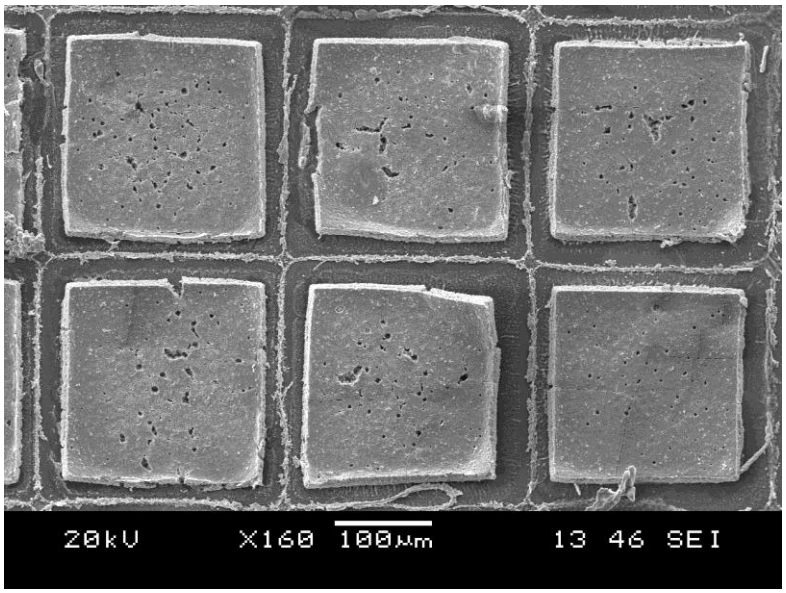

Figure 27 YSZ after EPD with colloid with PVA binder and subsequent sintering. Multiple cracks and burnout holes observed.

4.3.8 Carbon release layer

It was theorized that a layer of carbon between the sputtered Ni and deposited YSZ would reduce the adhesion between these two layers. In light of this several methods of creating a carbon release layer were explored, including a thin evaporated carbon layer, and carbon paint. None of these methods consistently worked, though on occasion several released membranes per sample were observed.

The first method tried was to spin carbon paint (05006, SPI) onto the sputtered Ni film. While the film looked smooth macroscopically, it was quite inhomogeneous when viewed under a microscope. Even the thickest films achieved (550nm) resulted in a carbon membrane with a resistance above 2MΩ, which was far too high for EPD to occur without assistance. However, the Ni film below the carbon was sufficiently conductive to allow EPD to occur on the carbon film. It was quite difficult, however, to pattern the SU-8 on the carbon paint, as adhesion of the SU-8 to the carbon was quite poor. Additionally, there was no way to spin the carbon on the samples after the patterning of the SU-8 for the obvious reason that the SU-8 walls would prevent the free flow of the carbon across the surface.

Regardless, the carbon paint proved to be a poor solution to the cracking problem, because, in addition to the above mentioned difficulties, the carbon caused catastrophic damage to the YSZ deposition as it burned out during the sintering process, as shown in Figure 28. Furthermore, the carbon release layer, when applied to samples with patterned squares, work a bit too well, causing the YSZ squares to completely lift off and float away (Figure 29).

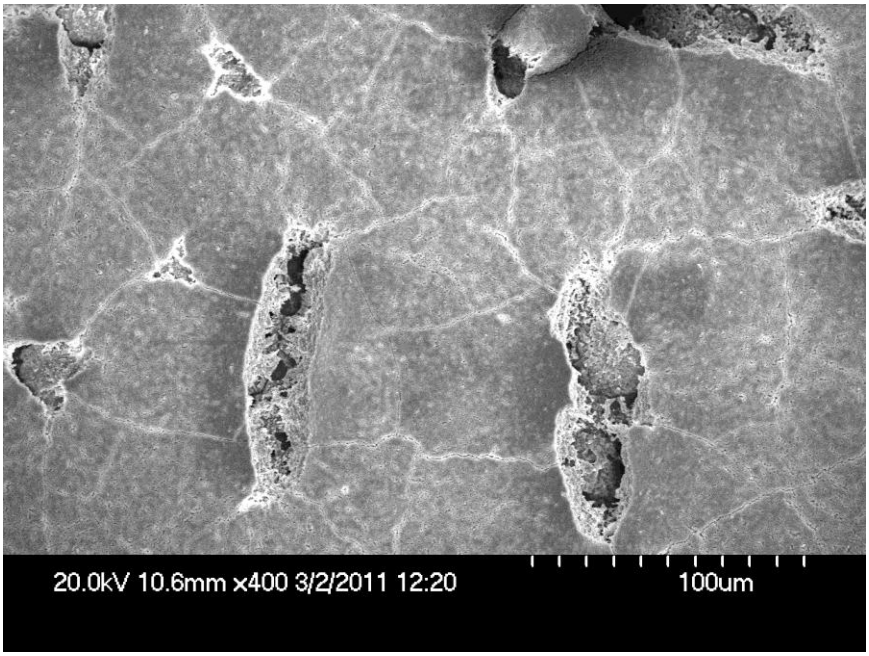

Figure 28 Surface of YSZ deposited on carbon paint layer after sintering. Carbon paint did not prevent cracking and causes further defects upon burning out.

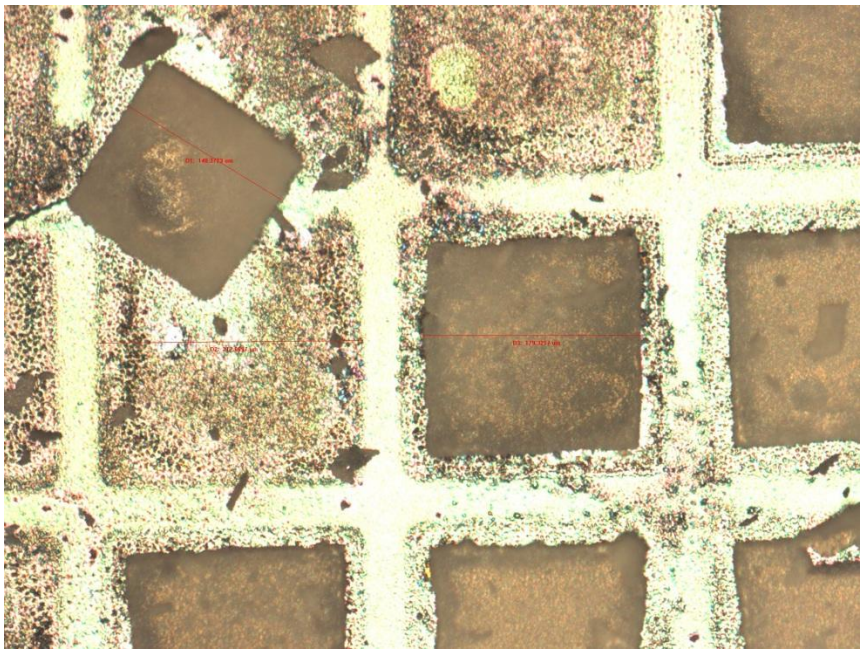

Figure 29 YSZ squares completely released by carbon paint layer.

Another method tried was to evaporate a very thin carbon layer from a carbon thread evaporator machine onto the Si dies with the sputtered Ni and patterned SU-8. This was also unsuccessful, as the carbon layer proved too thin to sufficiently lower the adhesion between the Ni and the YSZ (Figure 30).

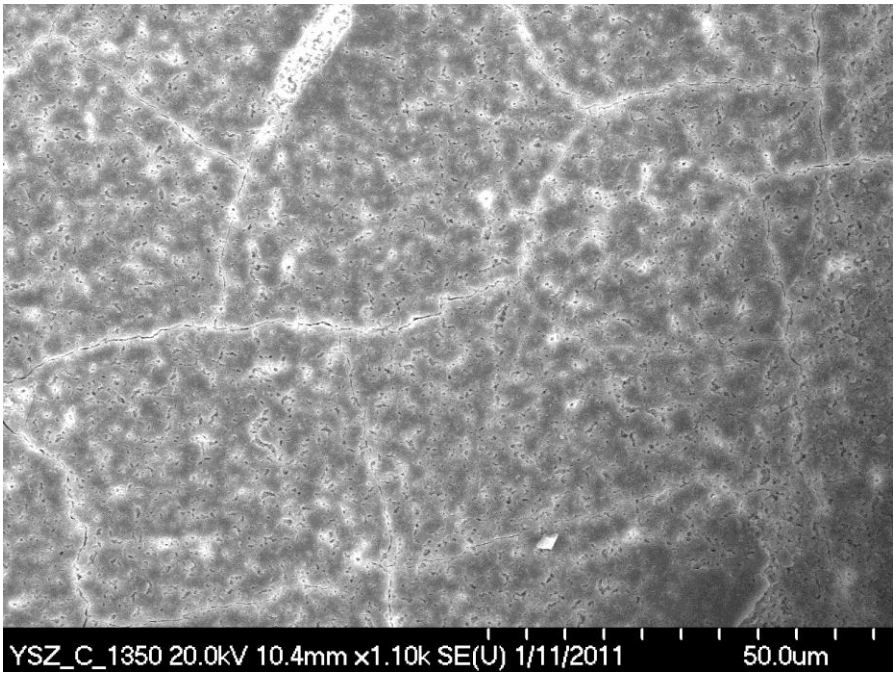

Figure 30 YSZ deposited on sputtered Ni with evaporated carbon layer, then sintered. Carbon layer did not prevent cracking or release membrane.

4.3.9 Flexible release layer

The final idea explored was to deposit the YSZ onto a layer which would melt at a low temperature, or just be flexible in general in the hopes that this would allow the YSZ to shrink freely. Two ideas related to this were tried though neither showed any success

The first idea was to try to deposit the YSZ directly onto a flexible PR layer. This idea never went anywhere, however, because the PR quickly dissolved away in the colloid mixture.

The second was to deposit an indium layer in between the Ni and YSZ layer. Given that indium melts at around 150°C, it was hoped that the liquid indium would allow the YSZ to freely shrink while being sintered. While a good idea in concept, it did not work, yielding a cracked,

porous deposit, as shown in Figure 31. This was likely due in part to a poor deposition on the indium layer to begin with. Furthermore, the indium balled up and seeped through the deposited YSZ (Figure 32).

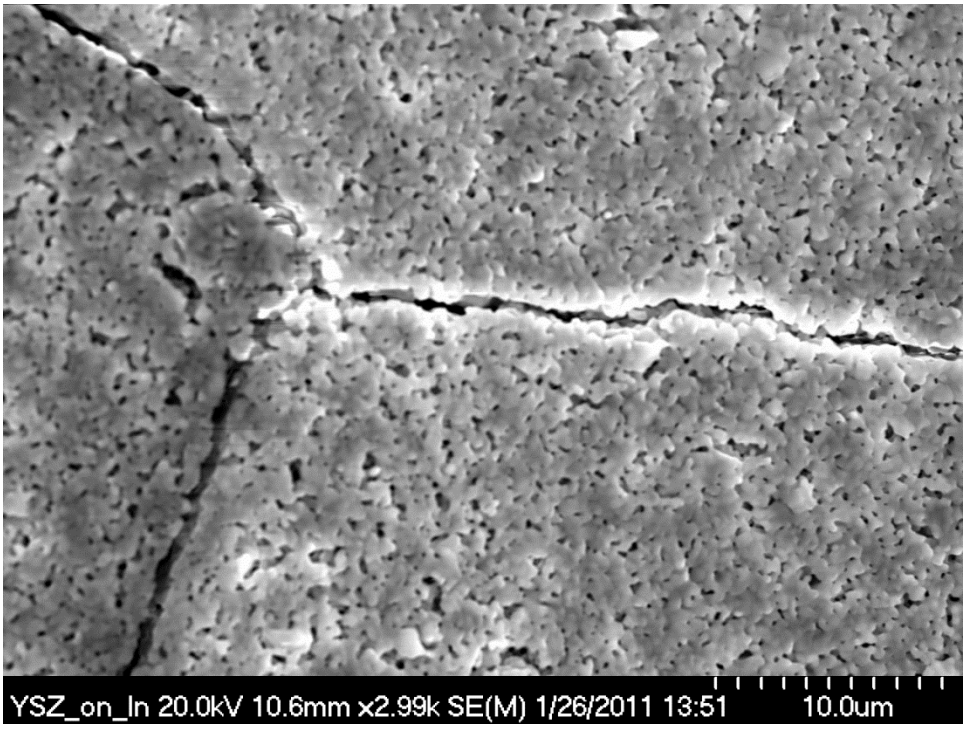

Figure 31 YSZ deposited on indium release layer, then sintered.

Figure 32 Indium release layer bubbling up through YSZ after sintering

4.4 YSZ-YSZ/NiO bilayer

Most of the work regarding achieving a YSZ membrane involved electrophoretically depositing the YSZ directly onto a sputtered Ni or Cr layer. Some work was done, however, to explore creating two of the membrane components, namely the porous anode, comprised of NiO and YSZ, and the dense electrolyte, comprised of YSZ in consecutive EPD depositions. A porous NiO/YSZ composite layer, which would serve as the anode for a fuel cell, was successfully created. However, the same shrinkage problems described above were experienced with the YSZ electrolyte layer, which continued to crack and remain porous upon sintering. This section will briefly describe additional processing steps taken while trying to achieve this anode-electrolyte bilayer.

A colloid containing both NiO (312010, FuelCellMaterials) and YSZ (TS-8Y, Tosoh) powders was prepared in a similar manner to the YSZ colloid described above. Again a mixture with 40% ethanol and 60% acetone was used, for the reasons described above. Iodine was again used as a surfactant, and a concentration of 0.5g/l was again used. The powder concentration of 1g/l was kept constant, but this time was a mix of YSZ and NiO powders. It was observed that there was a tradeoff between cracking and conductivity based on the ratio of NiO to YSZ. Because the NiO particles were somewhat larger than the YSZ particles, the deposited layers are more prone to cracking upon sintering. Therefore the ratio of NiO to YSZ must not be too high in order to prevent cracking. However, enough NiO must be present to achieve the adequate conductivity in the anode. According to literature, a mixture with 60% NiO and 40% YSZ balances this tradeoff [29]. The NiO and YSZ powders deposit at nearly the same rate over the times and voltages used, so a final composition of 60% NiO and 40% YSZ is expected in the deposit.

As before, the colloid components (solvent, surfactant, and powder) were placed in a glass container and then ultrasonicated for 2.5 hours, with vigorous shaking every 10-15 minutes to create a stable colloid. This was done simultaneously with a colloid containing only YSZ, and as such, the ultrasonic bath was again kept cool (5-20°C) with ice.

The samples were prepared on the Teflon holding plate as described above. Deposition occurred in two steps: the samples were first placed in the YSZ/NiO solution for 3 minutes with an applied potential of 30V, and then immediately transferred to the YSZ solution where a

potential of 120V was applied for 2 minutes. The required potential for the YSZ was higher than before due to the inherent buildup of resistance as the deposit gets thicker. It was observed that at the typical sintering temperature of 1400°C, the NiO film bubbled up and ruined the samples. Given this, a lower sintering temperature of 1190°C (for 3 hours, and with a ramp up time of 3 hours) was used. This prevented the destruction of the NiO film, but also did not allow the YSZ particles to properly sinter and become dense. Therefore, a bilayer was created, but both the YSZ/NiO and the YSZ layers were porous, as shown in Figure 33.

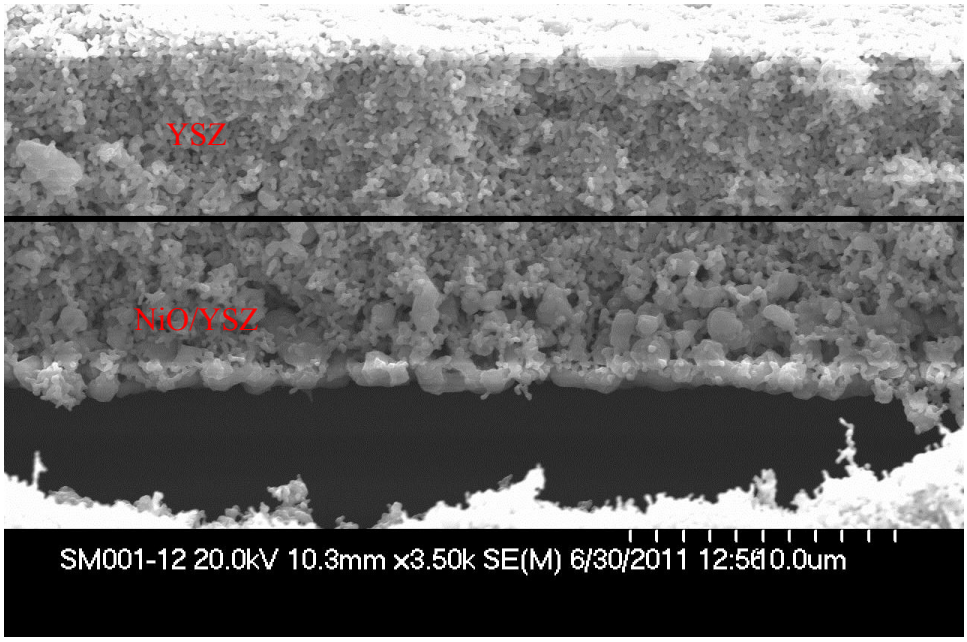

Figure 33 NiO/YSZ – YSZ bilayer via electrodeposition onto sputtered Ni

A NiO-YSZ composite porous composite layer for use as the anode was successfully created using electrophoretic deposition. However, the sintering temperature of 1400°C required to make the subsequently deposited YSZ layer dense caused the NiO to bubble and destroy the membranes. A lower sintering temperature of 1190°C prevented the destruction of the NiO layer, but as the cost of preventing the required densification of the YSZ layer. Given this inherent conflict with no apparent solution, NiO/YSZ-YSZ bilayers via EPD were not pursued further.

4.5 Conclusions

It was observed that cracking of the membranes can occur upon removal of the sample from the colloid and the evaporation of the solvents. However, this seems able to be prevented by using an acetone/ethanol colloid mixture and by drying the samples slowly in an acetone environment.

The bigger cause of cracking and low density in the YSZ membranes lies in the fact that they are unable to release and freely shrink while being sintered. It was confirmed that if properly released, a membrane would be allowed to shrink and become dense without cracking. However, this result was not repeatable, and most YSZ squares deposited on a sputtered metal layer showed strong adhesion. Subsequent attempts to allow the YSZ to release and become density without cracking, including polymer binders, a sacrificial carbon release layer, and a soft indium release layer proved ineffective. In all cases the attempted solution either caused further damage to the YSZ film (via burnout defects) or simply did not allow the YSZ to release.

It is thought, however, that if a consistent method of release could be achieved, EPD would prove to be a useful technique for creating printable YSZ membranes. One difficulty yet to overcome, however, would be to prevent the YSZ squares from completely floating away after being released. Additionally, a method for adding the porous anode and cathode layers to the electrolyte membrane would need to be devised.

Finally, although a bilayer containing NiO/YSZ- YSZ could be formed using subsequent deposition steps, the required sintering temperature of 1400°C to make the YSZ film dense caused the NiO powders to bubble up and destroy the deposited squares. A lower sintering temperature of 1190°C prevented the bubbling of the NiO, but also prevented the YSZ from becoming dense. This inherent conflict in the required sintering temperature was unable to be resolved, the creation of a bilayer with a porous NiO/YSZ layer and a dense YSZ layer was not achieved.

Chapter 5: EPD of Closed End Tubes

5.1 Intro

As mentioned before, EPD is a versatile process which can be used to create parts with complicated different geometries. Given this, an attempt was made to create closed end YSZ tubes for use in solid oxide fuel cells. The goal was to use EPD to create a dense closed end tube approximately 0.5mm in diameter and 0.75 mm long, and then paint on the anode and cathode layers. Although much effort was made, crack free tubes were never achieved. This chapter will briefly describe the efforts taken and the lessons learned.

5.2 EPD setup

A solvent based (40% ethanol, 60% acetone) colloid with 0.5g/l Iodine and 1g/l YSZ powder was created as described in the previous chapter. The preparation of the cathode was somewhat different, as a fundamentally different geometry was being attempted. 0.5" diameter carbon tubes (McMaster) were cut into 5/8" long sections. A 3/8" hole was then drilled 0.5" into the carbon using a standard drill bit. The carbon was sufficiently conductive to act as a cathode for EPD, though a SS wire was affixed to the carbon tube as shown in Figure 34 to allow the alligator clips from the power source to be connected. A SS steel rod was held in place in the middle of the carbon with a Teflon holder and acted as the anode. A schematic of this setup is shown in Figure 35.

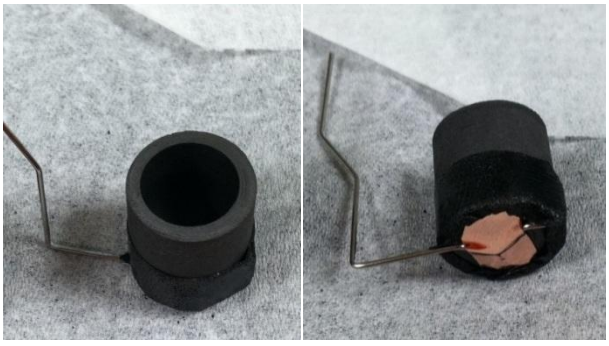

Figure 34 Carbon cathode for creation of closed end YSZ tubes via EPD

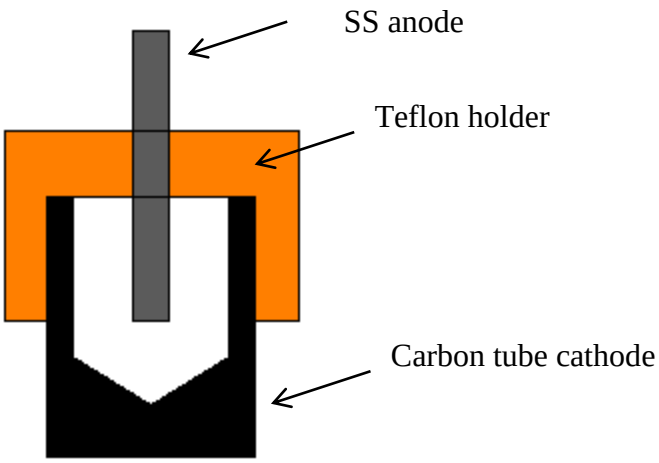

Figure 35 Cross-sectional schematic of EPD setup for closed end tubes

5.3 Deposition

For deposition, the entire apparatus (Teflon holder, SS anode and carbon cathode) was submerged into the prepared colloid. The Teflon holder has holes which allowed the colloid mixture to flow through and fill up the tube. However, given the small volume of the tube, manual mixing, which involved emptying and refilling the cavity was performed every minute during deposition. A deposition time of 20 minutes with an applied potential of 110V yield a 30um thick deposit on the inside of the carbon form. This voltage was significantly higher than that used for the YSZ membranes, because the carbon cathode was slightly less conductive, but more significantly, because as the membrane thickness increased, it greatly increased the resistance of the system.

Upon completion of the deposition, the carbon forms with the YSZ deposit were placed in an ethanol vapor environment, as described previously. The purpose of this was to allow the solvent to evaporate slowly to prevent cracking of the green deposit. However, given the increased thickness of the deposit, even these careful measures were unable to prevent cracking, even before the sintering step. Though much effort was taken, this cracking from initial drying could never be prevented. These cracks were then aggravated during the subsequent sintering

step. Given that the electrolyte is required to be gas impermeable, these crack tubes were unable to be used for fuel cell testing.

After deposition and drying, the carbon tubes with the YSZ deposit were place in a furnace in an oxygen atmosphere and sintered at 1400°C for 4 hours, with a ramp rate of 500°C/hour. At these temperatures the carbon completely oxidized, leaving only the sintered YSZ structure, as shown in Figure 36. This allowed the YSZ to shrink freely (about 30% shrinkage was observed) and become dense. However, although not macroscopically cracked, there was visible porosity in the bottom of the tubes, probably due to the complicated geometry, and the imperfect deposition given the limitations in the anode geometry. Furthermore, inspection with a microscope confirmed the presence of microcracks. The side walls were generally defect free, however, with the cracking and porosity being observed at the complicated geometry at the base of the tube. Figure 37 shows an SEM image of the fully dense YSZ membrane that was able to be achieved.

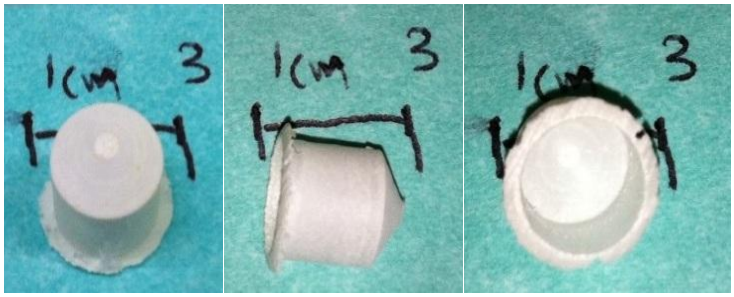

Figure 36YSZ closed end tube after being sintered at 1400°C

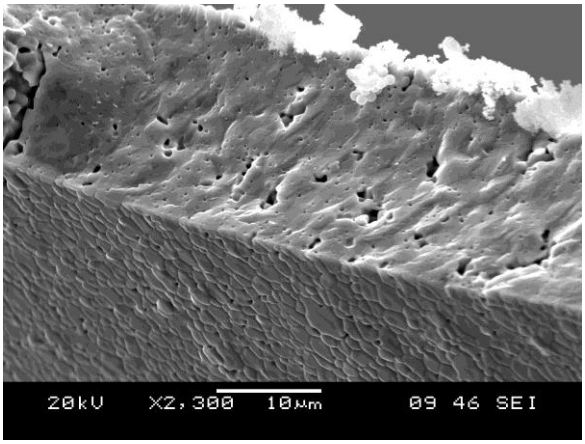

Figure 37 Fully dense YSZ film deposited via EPD

5.4 Anode-Electrolyte-Cathode

Although crack free tubes where not achieved, it is worth mentioning that a very nice anode-electrolyte-cathode structure was able to be created. After sintering, NiO (231001, FuelCellMaterials) paint was applied to the inside of the YSZ tubes and LSM paint (232101, FuelCellMaterials) was applied to the outside of the tubes. The tubes were then fired at 1100°C for 2 hours with a ramp time of 3 hours to cause the paint to dry. Although this further aggravated the cracking of the YSZ, membranes with a porous NiO layer, a dense YSZ layer, and a porous LSM layer were achieved, as shown in Figure 38

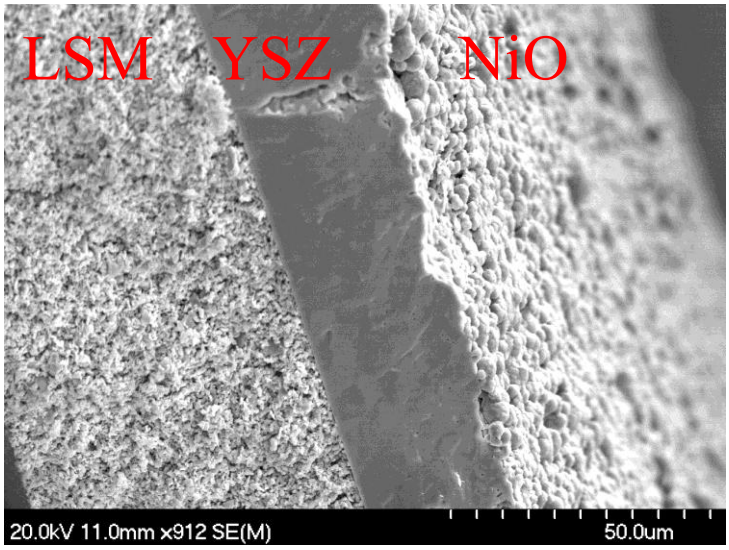

Figure 38 Membrane with porous LSM, dense YSZ and porous NiO layer

5.5 Conclusions

An attempt was made to create crack free closed end YSZ tubes via EPD. However, cracking during drying was unable to be prevented, event with slow drying in ethanol vapors. These cracks were aggravated during the subsequent sintering. In addition to this, the complicated geometry at the base of the tube always showed visible porosity after sintering, though it is unknown exactly what caused this. A porous LSM and NiO layer were achieved on the inside and outside of the tubes, respectively, yielding a composite membrane which locally looked very good. However the unavoidable microscopic cracking of the tubes during sintering rendered them unable to be used in SOFCs.

Chapter 6: Fabrication of YSZ membranes

6.1 Intro

The fabrication of the membranes is one of the most critical steps for successful transfer printing. Generally speaking, transfer printable membranes, or "inks" are created in an array on a silicon substrate. The array is then known as the donor substrate and the inks are then "printed" onto a receiving substrate. This section describes the processing steps taken to prepare 200 um square, 350 nm thick YSZ membranes with a 300 nm thick Ni backing layer for transfer printing.

6.2 Fabrication method

A schematic of the process used to fabricate the array of transfer printable YSZ inks is shown in Figure 39. A detailed description of the steps taken is given below:

a. A 2um thick layer of photoresist (AZ 5214) was spun onto a clean Si die at 2000rpm with a ramp rate of 1000rpm/s. The samples were then prebaked at 110°C for 1 minute to evaporate the solvents. The photoresist was exposed at 100mJ/cm^2, then reversal baked at 120°C for 2 min. The caused the exposed areas of the photoresist to crosslink so that a negative image of the mask, and hence a lift off profile, would be created. After the reversal bake, the samples were flood exposed (>200mJ/cm^2), developed in 1:4 AZ 351 solution for 40s, then dried with N_2.

b. A 10 nm Cr seed layer, followed by a 300 nm thick Cu sacrificial layer were deposited via DC magnetron sputtering with the AJA ATC Orion 8 HV series sputtering system in the Micro-Nano-Mechanical Systems (MNMS) cleanroom. The base pressure was below 1x10-7 Torr, and the sputtering pressure was maintained at 5mTorr, with 20 sccm Ar flow. A constant sputtering power of 300W was used for both metals and a sputtering time of 45 s and 12 minutes were used for the Cr and Cu layers, respectively.

c. A 300 nm thick Ni carrier layer was deposited via DC magnetron sputtering using the machine described above. A sputtering pressure of 5mTorr and 20sccm Ar flow were used. The power was 300 W and the sputtering time was 13 min, 45 seconds.

d. A 350 nm YSZ functional layer was deposited via RF sputtering. This step was far less straightforward and many problems were encountered before reproducibly sputtered films could be achieved. As such an in depth discussion of this step will occur later in this chapter.

e. The PR mask was lifted off by placing the samples in an acetone, and then ultrasonically cleaning them for 1 minute. This left an array of 200um square, 1 um thick metal/YSZ squares on the Si die.

f. 2 um thick PR (AZ 5214) anchors were patterned according to the processing steps described above. The purpose of these anchors was to hold the Ni/YSZ membrane in place after the Cu sacrificial layer was removed.

g. The Cu sacrificial layer was etched using Copper Etch BTP (Transene). This etchant is selective against Ni. The etch time varied slightly from ink to ink, with the first inks being fully undercut after 25 minutes. This step was rather tricky and will be covered in more depth later in the chapter.

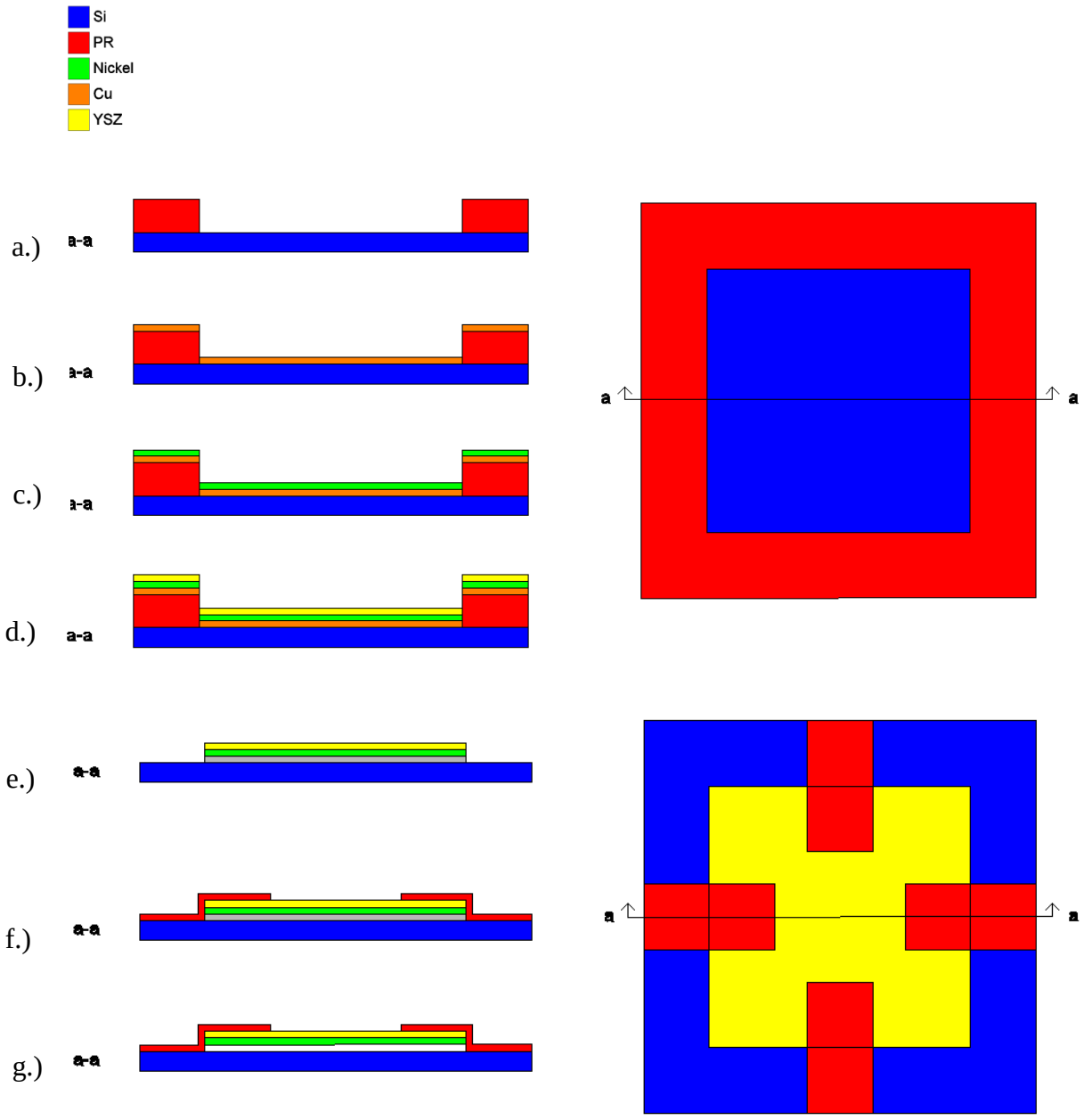

Figure 39 Schematic process flow of YSZ/Ni ink fabrication. a.) Pattern photoresist channels to mask out squares. b.) Sputter 300 nm Cu sacrificial layer. c.) Sputter 300 nm Ni carrier layer. d.) Sputter 250 nm YSZ functional layer. e.) Remove PR layer. f.) Pattern photoresist anchor. g.) Undercut Cu sacrificial layer.

6.2.1 Sputtering YSZ

The YSZ sputtering target (2" diameter) was placed into the chamber of the AJA 2 magnetron sputtering system in the Materials Research Laboratory (MRL). The distance from the target to the sample was approximately 6". The chamber was then allowed to pump down to $<4x\ 10^{-6}$ Torr to remove particles and water vapor from the system. Ar (20 sccm) was then introduced into the chamber. The chamber pressure was adjusted by controlling the amount that the gate covering the vacuum was open or closed. The chamber pressure was first adjusted to 30 mTorr so that a plasma could be struck on the target. Note that this was able to be done without the aid of an adjacent plasma, as is often the case for insulating targets. It was observed that an RF power of 20 W was sufficient to strike a plasma on the YSZ target. Upon striking of the plasma, the power was raised to 125W at a rate of 1 W/s to prevent the target from cracking from thermal stresses. After 125 W was reached, the deposition pressure was lowered to 1.5mTorr by manually opening the gate valve on the vacuum. This was done over the course of about 30s to prevent trauma to the plasma. A sputtering time of 90 minutes yielded a 350 nm thick film (based on surface profilometry), indicating a sputtering rate of 0.65Å/s (3.9nm/min). The YSZ sputtered on Ni exhibited columnar grain growth and is shown in Figure 40

According to the literature, a lower sputtering pressuring serves to increase the sputtering rate, though if the pressure is too low the plasma will not be sustainable. This is because the mean free path is increased at lower pressures, thus allowing the YSZ particles to travel more quickly and more directly from the target surface to the substrate surface. An in depth discussion of this and of other important parameters regarding sputtering YSZ can be found here [30] [31].

It should be noted that much time and effort were spent in getting sputtered YSZ films. While it is unknown for certain what all of the issues were, some theories are presented here. Firstly, the YSZ target purchased from AJA international was bonded to a backing plate, but did not have a ring holding the YSZ together. Therefore, after several uses, the target cracked. Of its own right this is not a problem. However, upon extended sputtering times, the target heated up, causing the indium to melt and short out the target and gun, thereby rendering a plasma impossible. A new YSZ sputtering target was acquired that had a bond ring around the YSZ to prevent it from cracking. This target still seemed to have trouble striking a plasma when used in AJA 1 in MRL, though this could be due to a short in the gun, or some other unknown error.

Regardless, when used on gun 1 in AJA 2 in MRL according to the parameters described above, reproducible sputtering results were able to be achieved.

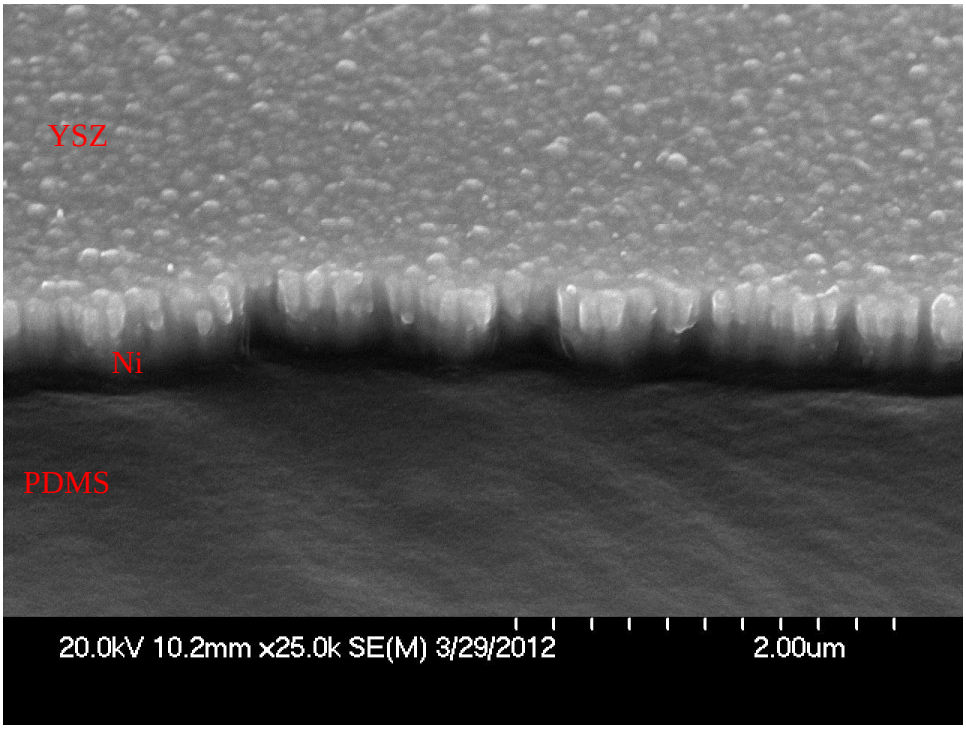

Figure 40 Sputtered YSZ film on Ni carrier layer

.

6.2.2 Membrane release

One of the trickiest steps in the process is the removal of the Cu layer to release the Ni/YSZ membranes. The problem lies in the fact that upon removal of the Cu layer, many of the Ni/YSZ membranes bent and broke the PR anchors. The cause of this is unknown as it is not expected that there would be either a compressive or tensile thermal stress between the Ni and YSZ, since they were both sputtered at room temperature.

Given that the Cu sacrificial layer was exposed on all sides, the Cu etched inward from all directions. Eventually, the Cu became relatively circular, with the radius of the circle decreasing as the etching continued. However, the Ni layer prevented this from being visually observed, so it was difficult to gauge the progress of the undercutting. The exact etch rate varied

from ink to ink, with the first inks being completely undercut after 25 minutes, as indicated by the fact that some of them broke the PR anchors and floated away. It was noted that upon removal from the etchant, the Ni/YSZ membranes sometimes sagged around the remaining Cu on the inks that were not completely undercut. The sagging created a physical barrier which prevented the Cu etchant from reaching the remaining Cu and completing the undercut.

An optical image of the inks after the removal of the Cu layer is shown in Figure 41. Note that in the 4 x 6 array shown, 15 inks did not break the PR anchors and float away, giving a local yield of about 60%. As mentioned, however, some of the inks were not able to be fully undercut due to the problem discussed before. Also, the edges of the sample had a lower yield. Therefore the overall ink yield is estimated to be about 20%, though it is assumed that further refinement of the etching process will cause much higher yields.

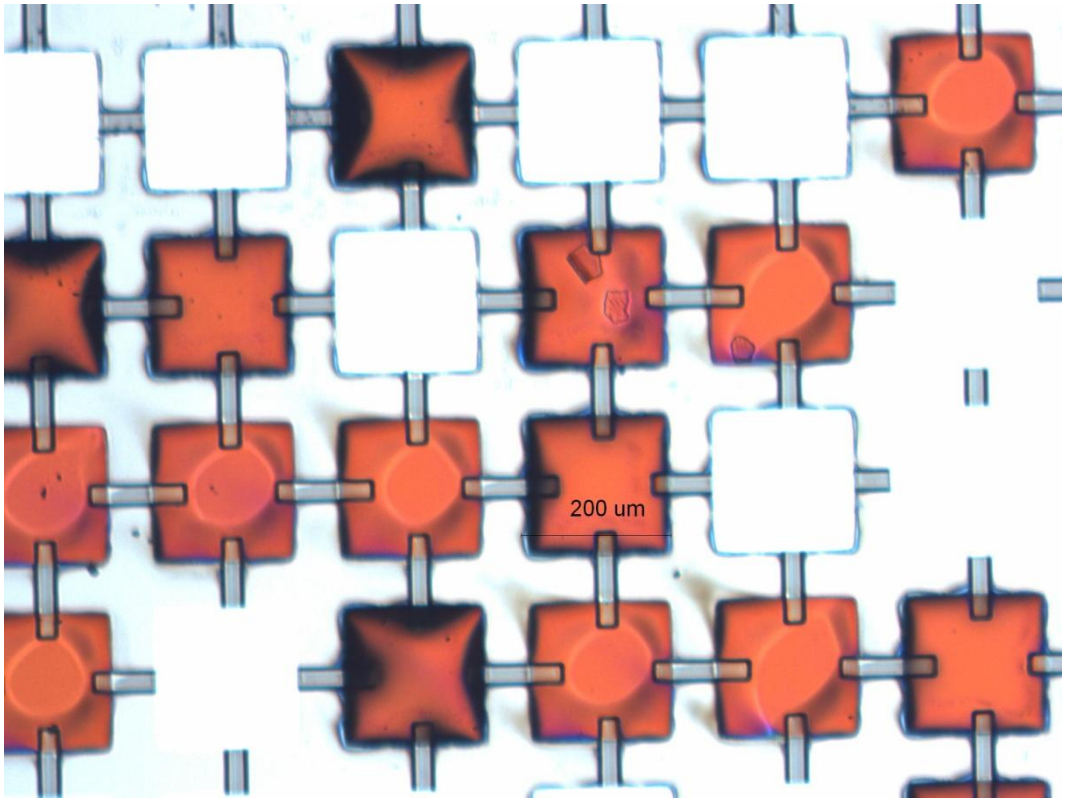

Figure 41 Array of Ni/YSZ inks after removal of the Cu sacrificial layer.

6.3 Additional fabrication paths

In addition to the above mentioned method of using PR anchors to support the inks, and idea based on the directional etching of <111> Si was also developed. The general premise behind this idea is to deposit the Ni/YSZ layers directly onto the silicon, then undercut the silicon below the membranes. The membranes would be supported via tabs which would connect to Ni/YSZ that was not undercut. A schematic diagram of this concept is shown in Figure 42, with general processing steps being given below:

a. Pattern 2um thick photoresist layer (AZ 5214) according to standard photolithography techniques.
b. Sputter the required membrane layers: Ni, YSZ and LSM.
c. Remove the PR mask, leaving an array of squares connected to parallel supporting pillars by small tabs
d. RIE etch 1 um into Si
e. Directional KOH etch to undercut membranes.

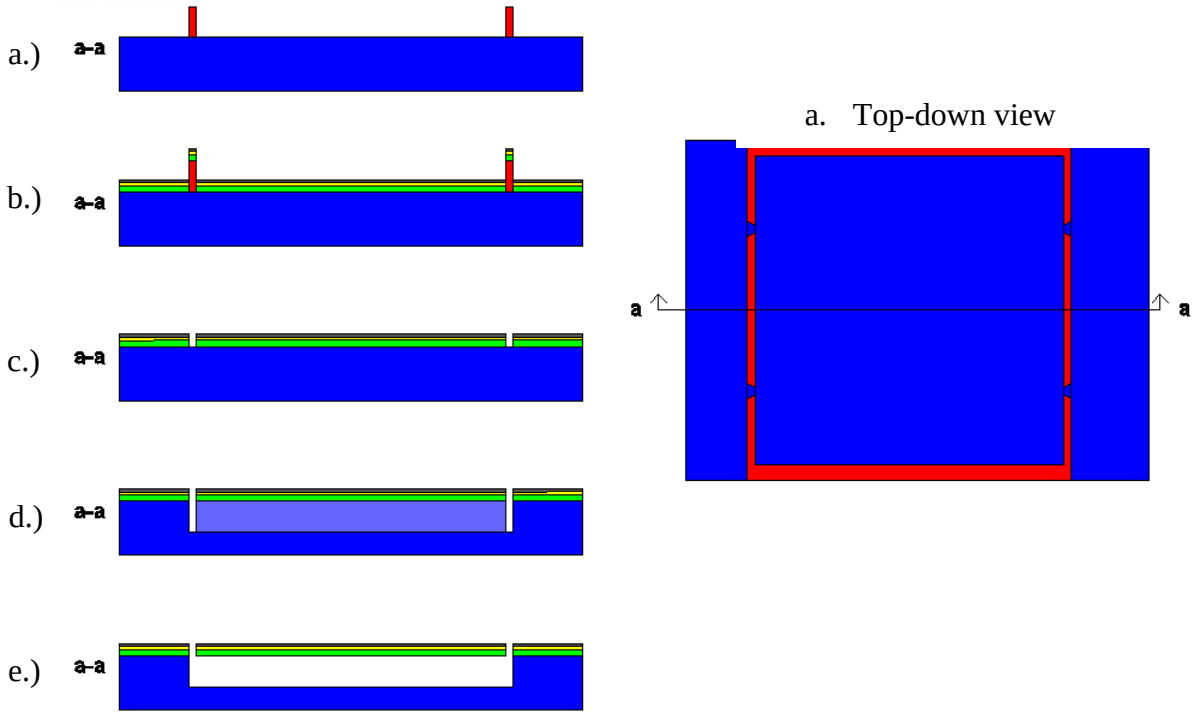

Figure 42 Schematic of creation of printable Ni/YSZ membranes based on <111> directional etching.

6.4 Porous Anode/Cathode

As mentioned previously in this thesis, a functional fuel cell membrane requires a porous anode and cathode layer in addition to the dense electrolyte layer. Dense YSZ membranes have been formed, but a complete membrane electrode assembly has not yet been achieved.

It was mentioned that Ni is the most commonly used anode material and that LSM is the most commonly used cathode material. However, this is only true for larger scale fuel cells. Review of literature shows that Pt is almost exclusively used as the anode/cathode layer for ultrathin membranes such as the ones we are creating [2]. It is assumed that this is because of the inherent difficulty in creating porous Ni and LSM films which are also compatible with the ultrathin (300nm) YSZ electrode used. A review of literature showed that there is no simple way of creating extremely thin, porous LSM or Ni films. However, it seems that it is possible to create a 60-80 nm porous Pt film simply by modifying the sputtering conditions [2] [4] [32].

Therefore, it is suggested that Pt be used for the cathode layer. This would not significantly change the process flow defined above as it would simply add another deposition step after the YSZ deposition, but before the PR is removed.

The anode layer presents slightly more concern. While a porous Pt layer could be deposited, it is unknown whether or not the YSZ will be able to be sputtered on the porous Pt. More significant is the question of whether or not the Pt layers would be sufficient to protect the YSZ from cracking during the transfer printing step.

Another idea is to deposit the Ni as specified above. After the membranes have been printed, they would be heated in an oxygen environment, causing porous NiO to form. The NiO would be reduced in situ to Ni during regular fuel cell operation [1].

6.5 Conclusions

An array of 200um square, 650nm thick Ni/YSZ membranes have been prepared for transfer printing using standard microfabrication techniques. These membranes are held in place by PR anchors after the sacrificial Cu layer is etched away. It was noted that upon release, some of the membranes bent, broke the PR anchors and floated away. 20% overall yield was

achieved (with locally much higher yields seen), but it is assumed that refinement of the etching process, either by the use of stronger anchors or more careful etching will allow higher ink yields to be possible. Another fabrication method using <111> Si etching was suggested, but has not yet been confirmed to work. Finally, there is a need for the porous anode and cathode layers to be added to the YSZ membrane. Pt is the most commonly used material, though the cost of platinum makes this prohibitive. More research is required to generate a method for creating porous Ni and LSM films at that scale level, however.

Chapter 7: Transfer Printing of YSZ membranes

7.1 Intro

The most important aspect of this thesis is the fact that transfer printing of the YSZ membranes has been successfully demonstrated. Although more work is required to finalize the ink design, especially with regard to the porous anode/cathode, the fact that these membranes are able to be heterogeneously transfer printed without cracking opens a world of possibility for the future of fuel cells. This is because membranes can now be fabricate independently of the support structure, and then transfer printed in place. This greatly simplifies the processing required to microfabricate the membranes and the fuel cell structure simultaneously.

7.2 Overview of transfer printing

Transfer printing allows microscale devices to be very precisely combined. This process is being researched and developed at the University of Illinois as a groundbreaking tool for microfabrication. The basic concept of transfer printing is to pick up a device ("ink") from a donor substrate, then place ("print") it on a receiving substrate. Specifically, research is being done on adhesionless transfer printing, which refers to the fact that no adhesive is applied to the receiving substrate to aid in the transfer of the ink.

According to Figure 43, the first step is to bring the polydimethylsiloxane (PDMS) stamp into contact with the devices to be transferred (Figure 43a). PDMS is a viscoelastic material which has high Van der Waals adhesion to most materials. This adhesion is enough to cause the devices to stick to the stamp, as gravity is insignificant at this scale (10s to 100s of microns). After contact, the devices are lifted off the donating substrate. In order for lift off to happen, the adhesion force between the stamp and the device must exceed the adhesion force between the device and the donor substrate (Figure 43b). This is accomplished by quickly pulling the stamp back from the donor substrate.. The next step is to use the PDMS stamp to move the devices to the receiving substrate (Figure 43c) and then "print" them to the substrate (Figure 43d). Printing is done by reversing the pickup process; the devices are brought in contact with the receiving substrate, then the stamp is removed. Similar to before, this can only be accomplished if the adhesion forces between the substrate and the device exceed the adhesion forces between the stamp and the device. In order to print the devices, the PDMS is slowly pulled back from the receiving substrate to allow the device to have time to delaminate from the stamp. A full

discussion of transfer printing is beyond the scope of this thesis but is available elsewhere in literature [9] [8] [7].

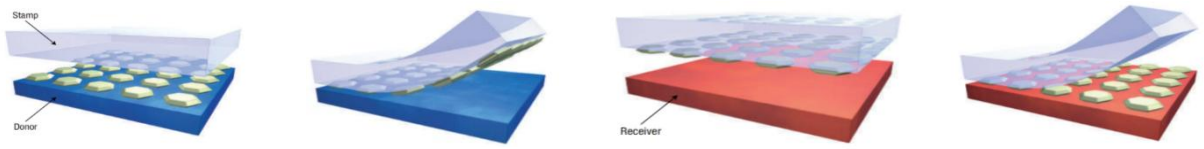

(a) Prepare donor substrate; apply rubber stamp

(b) Quickly peel-back stamp; grab objects off of donor

(c) Apply inked stamp to receiving substrate

(d) Slowly peel-back stamp; print objects

Figure 43 Generic schematic of transfer printing [7]

7.3 Transfer printing of YSZ membranes onto PDMS

An array of YSZ membranes was prepared according to the process flow described in the section above. The only change is that no Ni was deposited, yielding YSZ only membranes as shown in Figure 44. These membranes were then transfer printed onto a PDMS receiving substrate with a PDMS stamp. There was a 100% pickup and print rate, but 15 of the 16 printed stamps were noticeably cracked, as seen in Figure 45. Notice, however that the membranes in Figure 44 are visibly warped. It is thought that when the PDMS stamp was brought into contact with the YSZ membranes, that the warping was compressed, causing the membranes to crack. Furthermore, the trauma encountered in breaking the PR anchors probably also caused cracking.

It is useful to note, however that transfer printing crack free YSZ membranes is possible, as shown in Figure 46. However, the fact that most membranes cracked during the printing process suggested the need to implement some sort of a flexible carrier layer to prevent the brittle YSZ membranes from cracking. In light of this a Ni carrier was implemented, as discussed in the next section.

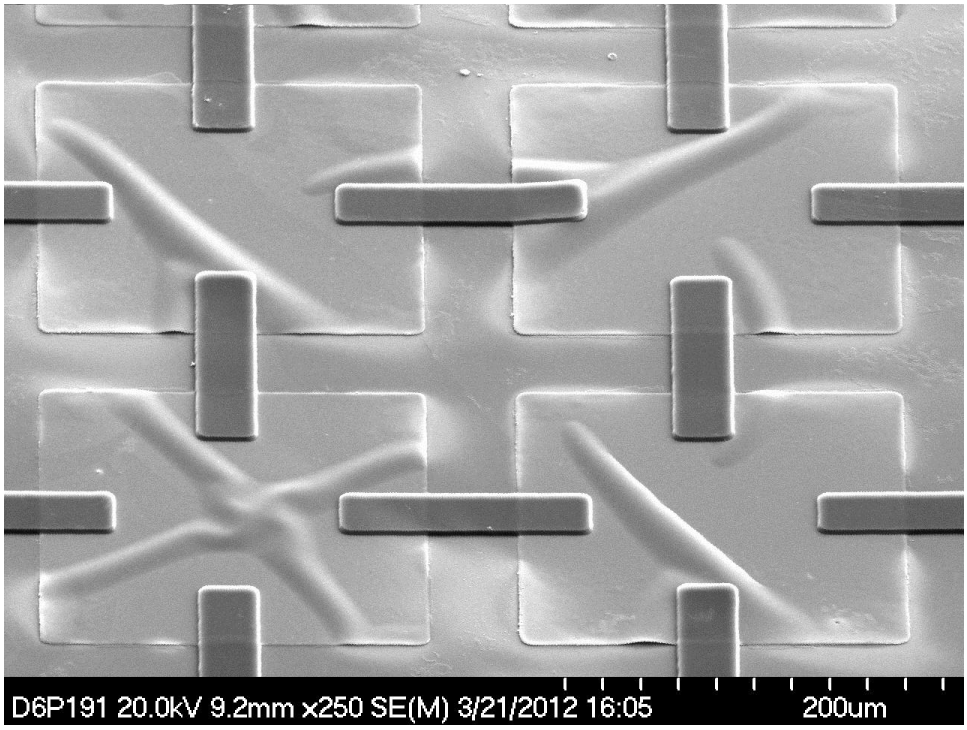

Figure 44 Array of 350 nm YSZ membranes ready for transfer printing

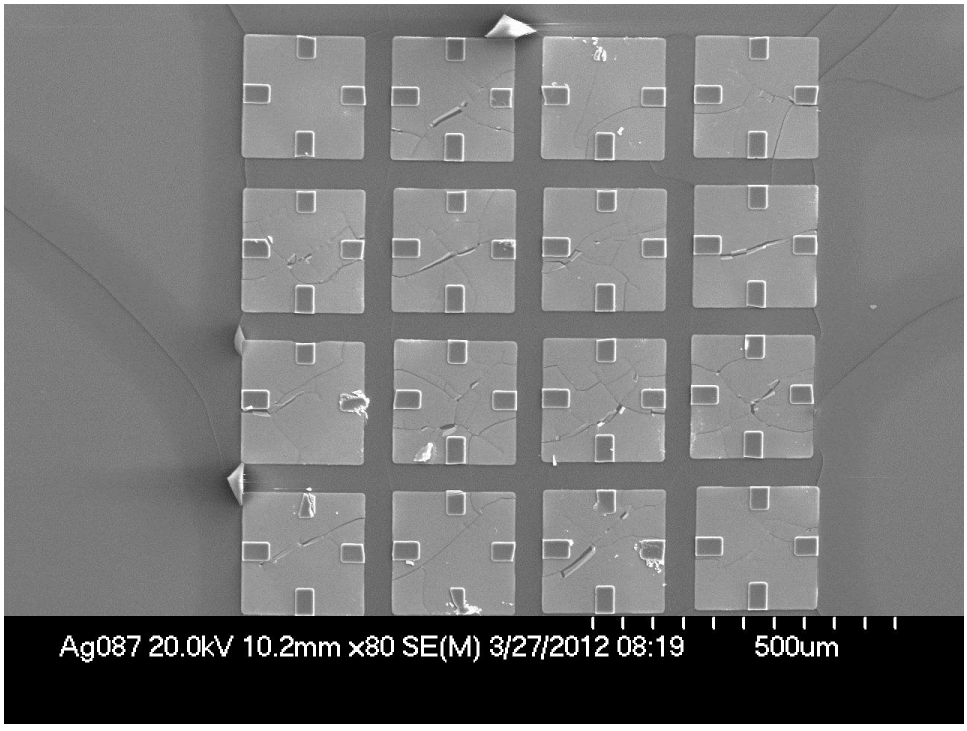

Figure 45 350nm YSZ membranes transfer printed onto PDMS

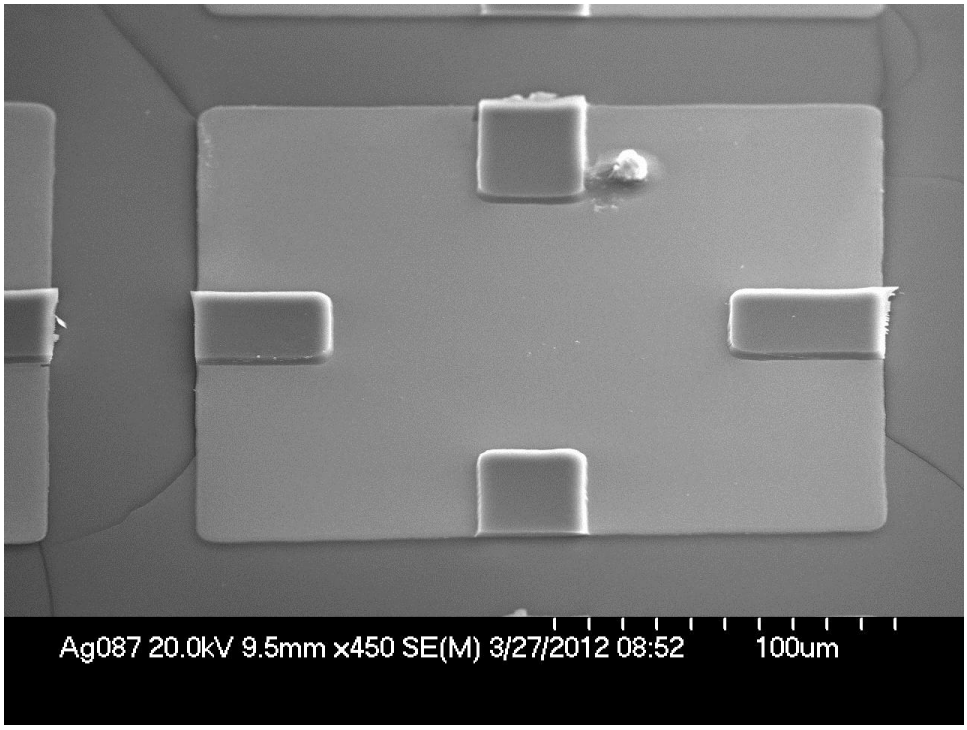

Figure 46 Crack free YSZ membrane transfer printed onto PDMS

7.4 Transfer printing of Ni/YSZ membranes onto PDMS

An array of 200um square, 650nm thick Ni/YSZ membranes were fabricated as described in the previous chapter. This substrate was used as the donor substrate for the subsequent transfer printing. A 200um square PDMS post was used to pick the membranes up from the donor substrate (Figure 47) and print them onto a PDMS receiving substrate (Figure 48). Although the ink itself had poor yield, the transfer printing yielded a 100% pickup and print success rate for the 16 inks printed. It is assumed that the surface adhesion energy between the Ni and PDMS exceeds that of the YSZ and PDMS, which is why the membranes were able to show a 100% print rate.

Additionally, the PR anchors were sufficiently weak to break without destroying the membranes. After transfer printing, the remaining PR residue on the membranes would need to be cleaned off. This can be done by placing the samples in an O_2 plasma, which attacks the organic PR, but leave the YSZ membrane unaffected.

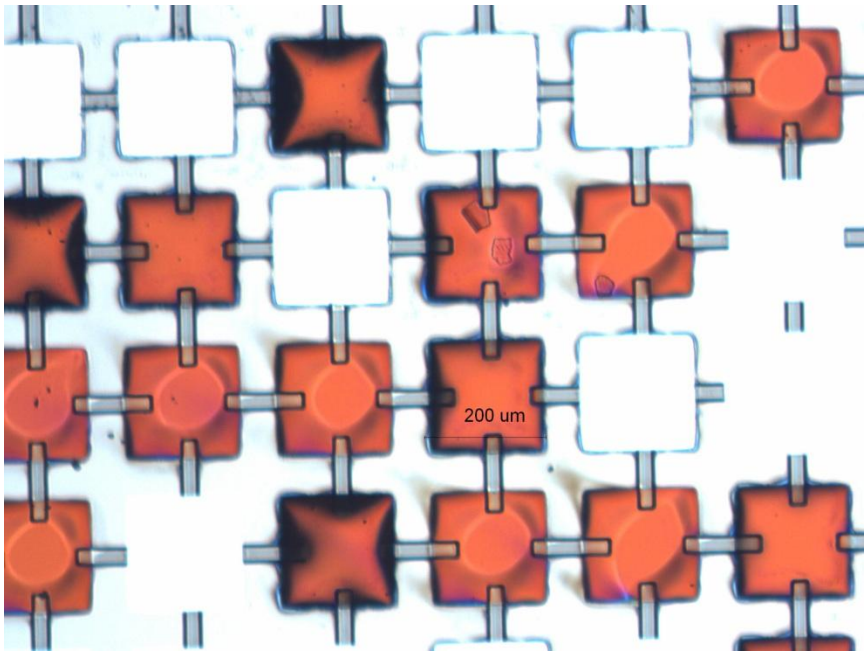

Figure 47 YSZ donor substrate

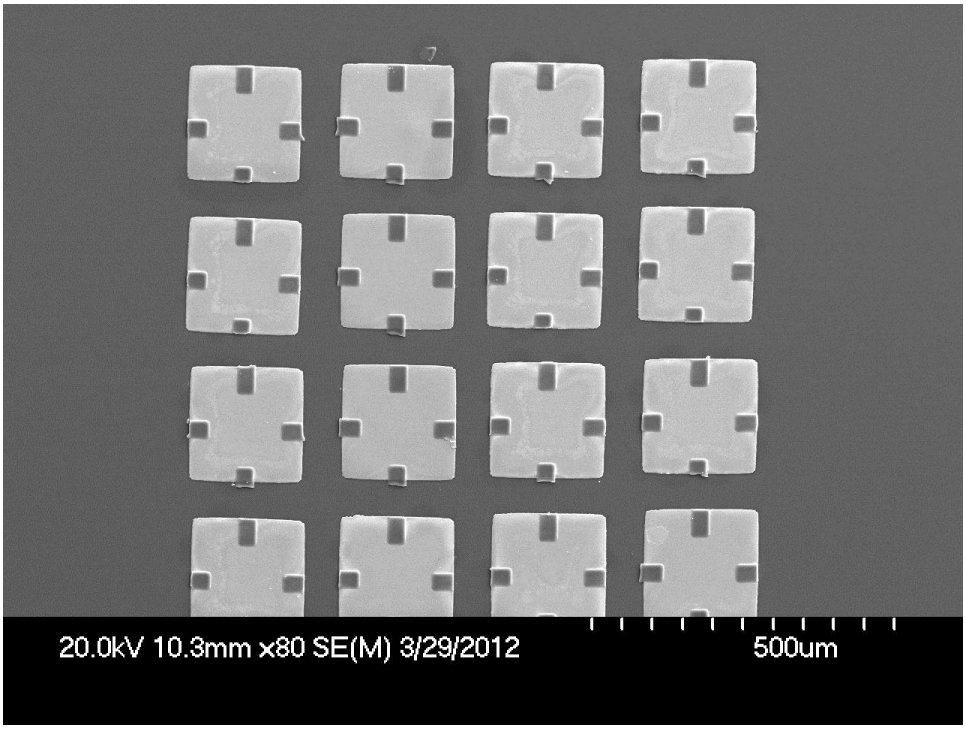

Figure 48 Array of crack free Ni/YSZ membranes transfer printed onto a PDMS substrate

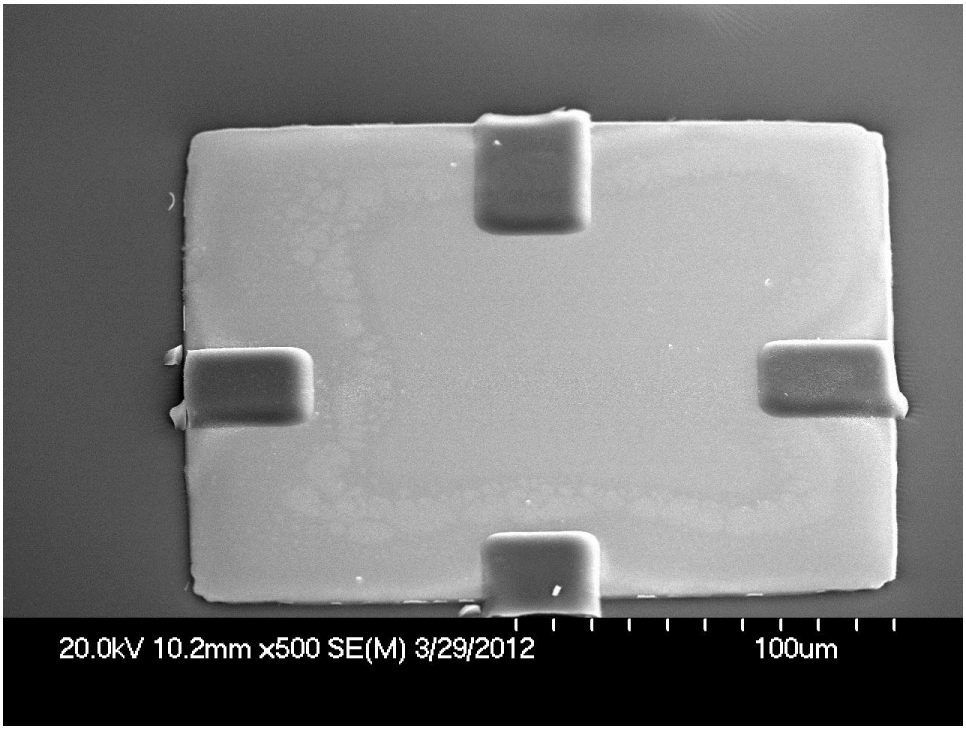

Figure 49 Crack free Ni/YSZ membrane transfer printed onto a PDMS substrate

7.5 Transfer printing of YSZ membranes onto Si

Although the ability to print YSZ membranes on PDMS is instructive, it does not account for the fact that the fuel cell design proposed requires the YSZ membranes to be printed on a silicon structure. In light of this, it was demonstrated that Ni/YSZ membranes could be printed onto a silicon structure similar in nature to that in the proposed design. In order to do this, however, special measures had to be taking in the printing process. This is because the adhesion of most materials to PDMS is generally higher than the adhesion to silicon. Therefore, it is difficult or impossible to transfer the Ni/YSZ membrane to the receiving substrate because of its preferential adherence to the PDMS stamp.

This difficulty was overcome by using a microtip PDMS stamp to print the membranes. A schematic of this concept is shown in Figure 50. Basically, the microtips deform, allowing the larger surface of the stamp to adhere to the ink for pick up. After the ink is on the stamp, the bulk area of the stamp relaxes from the ink surface, so that the ink is only being held by a very small area of contact on the microtips. In this way, the ink may be printed onto a receiving

substrate with a lower adhesion, because the area of contact will be greater. A full explanation of this process is available in literature [33].

Silicon frames (250 µm squares, 3um thick) were transfer printed onto a PDMS receiving substrate using a 200 µm square PDMS post. The Ni/YSZ membranes previously described were then transfer printed onto the silicon frames in such a manner that the bulk of the YSZ was exposed on both sides, with just the edge of the ink making contact with the silicon, as required by the proposed fuel cell stack design. This was accomplished by use of a microtip patterned PDMS stamp. An SEM image of the silicon frame and the Ni/YSZ membrane printed on the frame is shown in Figure 51. The ultrathin membranes were again able to be printed without cracking.

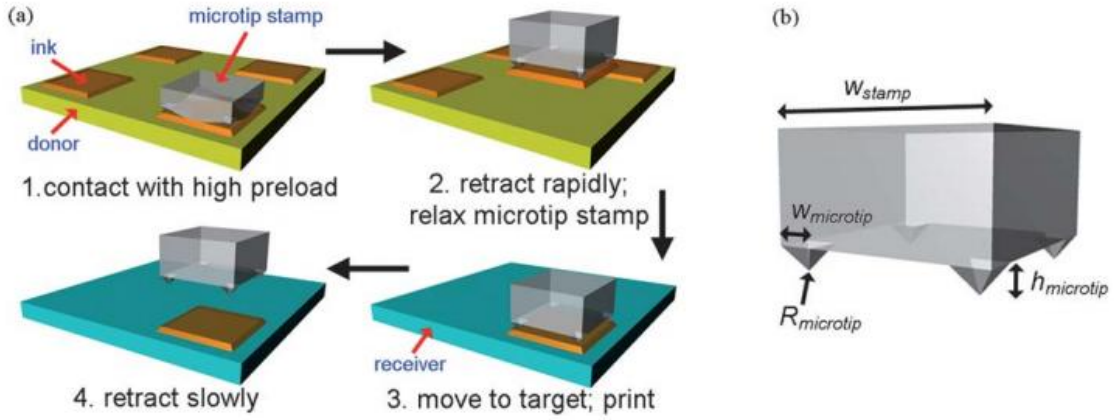

Figure 50 (a) Implementation of elastomeric, microtip adhesive surface in a stamp for deterministic assembly by transfer printing. (b) Elastomeric, microtip adhesive surface consisting of four features of microtip relief on the surface of square post. [33]

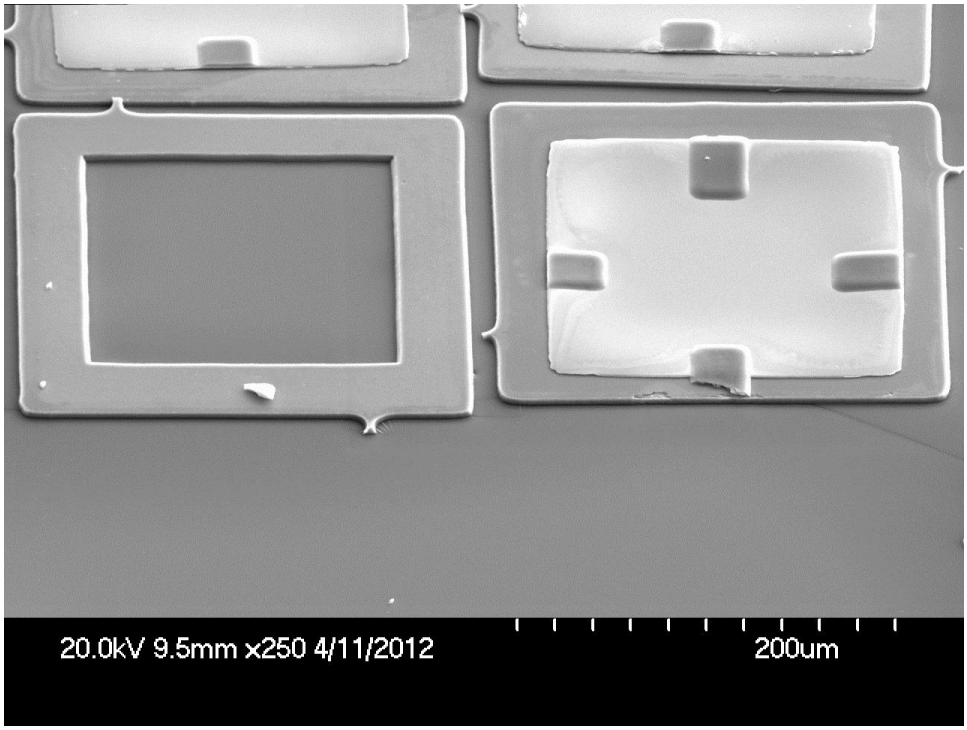

Figure 51 (left) 3um thick silicon frame. (right) ultrathin Ni/YSZ membrane printed onto silicon frame

7.6 Conclusions

It has been demonstrated that crack free ultrathin YSZ and Ni/YSZ composite membranes can be fabricated on a silicon substrate using standard micrfabrication techniques. The YSZ membranes were transfer printed onto a PDMS substrate, but became cracked in the process. To prevent against this cracking, a Ni carrier layer was introduced to the membrane. These Ni/YSZ composite membranes were able to be transfer printed onto a PDMS substrate without cracking. More significant is the fact that these Ni/YSZ membranes were able to be printed onto a silicon frame, as required by the proposed fuel cell design. Though work remains to develop the actual fuel cell stack, this result demonstrates that the fundamental processing steps required for the fuel cell are indeed feasible.

Chapter 8: Conclusions and Recommendations

8.1 Conclusions

A general concept for a μSOFC based on transfer printing was developed. Basic modeling was done to show the feasibility of such a cell, in terms of its thermal sustainability, and the required flow pressures. The first steps towards the actual construction of such a cell were then taken.

Ultrathin (350 nm) crack free YSZ membranes were fabricated on a silicon die and were successfully transfer printed onto a PDMS receiving substrate. While some crack free printed membranes were achieved, most of the membranes cracked during the transfer printing process. This was because the membranes warped upon release from the donor substrate and cracked when the PDMS was brought in contact with the inks for printing.

Crack free ultrathin (650 nm) Ni/YSZ composite membranes for use in μSOFCs were successfully fabricated on a silicon die using standard microfabrication techniques. The addition of the Ni carrier layer made the inks much less prone to cracking. These membranes were then successfully transfer printed onto a PDMS receiving substrate. All of the printed membranes were crack free, thus demonstrating that transfer printing is a viable technology for the manipulation of YSZ functional membranes for use in μSOFCs. Furthermore, these membranes were transfer printed onto a silicon support structure, thereby demonstrating the feasibility of the assembly steps required by the proposed cell design and taking the first steps toward the creation of a functional μSOFC based on transfer printing.

8.2 Recommendations

There are still many challenges to overcome before a functioning μSOFC based on transfer printing is achieved. First, a fabrication method for a complete MEA still needs to be worked out. The current inks have a dense Ni layer with a dense YSZ layer, but a functional MEA requires a porous Ni (or other anode material) layer, a dense YSZ layer and a porous LSM (or other cathode material) layer. Porous platinum layers for use as the electrodes may be achieved relatively easily via sputtering. However, the cost of platinum makes this solution prohibitive, so it would be better to achieve porous Ni and LSM layers.

After the membrane design has been finalized, there is also work do be done with regard to the fuel cell structure itself. This thesis presents a rough sketch of how the fuel cell structure, particularly the Si interconnect structures, should look. More design work, especially related to the specific processing steps required, is needed to define exactly how to build the Si interconnect structure.

Upon completion of the membranes and Si interconnects, the next step is to iron out the details regarding how to actually assemble the fuel cell. It has been demonstrated in this thesis that transfer printing is a viable method for placing the membranes on the Si structures. However, other processing steps, such as how to remove the PR anchors from the membranes, how to seal the membranes to the Si and how to seal the entire fuel cell still need to be worked out.

Furthermore, a method for keeping the heat in the fuel cell, such as an insulating coating or a heat exchanger for the gases should be devised. Rough calculations showed that heat loss does not appear to be an issue, but it is thought that further modeling and analysis is required to understand the exact heat characteristics of the fuel cell. Keeping heat in and maintaining the required operating temperature is critical to high efficiency operation, so a careful analysis of this should be done.

The ability to transfer print YSZ membranes opens a world of possibility for the future of fuel cells. While there are details yet to be worked out, this assembly method bridges the gap in literature between the construction of individual membranes and the need to build functioning fuel cells. Transfer printing paves the way for the construction of an actual high power density μSOFC as it makes many new design options possible.

References

1] R. M. Ormerod, "Solid Oxide Fuel Cells," *Chem. Soc. Rev.,* vol. 32, pp. 17-28, 2003.

2] A. Evans, A. Bieberle-Hutter, J. L. M. Rupp and L. J. Gauckler, "Review on microfabricated micro-solid oxide fuel cell membranes," *J. of Power Sources,* vol. 194, pp. 119-129, 2009.

3] A. Evans and e. al., "Micro-solid oxide fuel cells: status, challenges and chances," *Monatsh chem,* vol. 140, pp. 975-983, 2009.

4] H. Huang, M. Nakamura, P. Su, R. Fasching, Y. Saito and F. B. Prinz, "High-Performance Ultrathin Solid Oxide Fuel Cells for Low-Temperature Operation," *J. of the Electrochemical Society,* vol. 154, no. 1, pp. B20-B24, 2007.

5] R. Doshi, V. L. Richards, J. D. Carter, X. Wang and M. Krumpelt, "Development of Solid-Oxide Fuel Cells That Operate at 500°C," *Journal of the Electrochemical Society,* vol. 146, no. 4, pp. 1273-1278, 1999.

6] P.-C. Su, C.-C. Chao, J. H. Shim, R. Fasching and F. B. Prinz, "Solid Oxide Fuel Cell with Corrugated thin Film Electrolyte," *Nano Letters,* vol. 8, no. 8, pp. 2289-2292, 2008.

7] M. A. Meitl, Z.-T. Zhu, V. Kumar, K. J. Lee, Z. Feng, Y. Y. Huang, I. Adesida, R. G. Nuzzo and J. A. Rogers, "Transfer printing by kinetic control of adhesion to an elastomeric stamp," *Nature Materials,* vol. 5, pp. 33-38, 2006.

8] T.-H. Kim, A. Carlson, J.-H. Ahn, S. M. Won, S. Wang, Y. Huang and J. A. Rogers, "Kinetically controlled, adhesiveless transfer printing using microstructured stamps," *Applied Physics Letters,* vol. 94, p. 113502, 2009.

X. Feng, M. A. Meitla, A. M. Bowen, Y. Huang, R. G. Nuzzo and J. A. Rogers,

9] "Competing Fracture in Kinetically controlled Transfer Printing," *Langmuir,* vol. 23, pp. 12555-12560, 2007.

10] L. Besra and M. Liu, "A review on fundamentals and applications of electrophoretic deposition (EPD)," *Progress in Materials Science,* vol. 52, pp. 1-61, 2007.

11] L. Jia, Z. Lu, X. Huang, Z. Liu, K. Chen, X. Sha, G. Li and W. Su, "Preparation of YSZ film by EPD and its application in SOFCs," *Journal of Alloys and Compounds ,* vol. 424, pp. 299-303, 2006.

12] L. Besra, C. Compson and M. Liu, "Electrophoretic deposition on non-conducting substrates: The case of YSZ film on NiO-YSZ composite substrates for solid oxide fuel cell application," *Journal of Power Sources,* vol. 173, pp. 130-136, 2007.

13] S. M. Haile, "Swiss Rolls and Oreo Cookies," *Engineering & Science ,* vol. 1, pp. 18-27, 2003.

14] T. Suzuki, T. Yamaguchi, Y. Fujishiro and M. Awano, "Fabrication and characterization of micro tubular SOFCs for operation in the intermediate temperature," *Journal of Power Sources ,* vol. 160, pp. 73-77, 2006.

15] T. Suzuki, Y. Funahashi, T. Yamaguchi, Y. Fujushiro and M. Awano, "Design and Fabrication of Lightweight, Submillimeter Tubular Solid Oxide Fuel Cells," *Electrochemical and Solid-State Letters,* vol. 10, no. 8, pp. A177-A179, 2007.

16] T. Suzuki, Y. Funahashi, T. Yamaguchi, Y. Fujishiro and M. Awano, "Cube-type micro SOFC stacks using sub-millimeter tubular SOFCs," *Journal of Power Sources,* vol. 183, pp. 544-550, 2008.

17] T. Suzuki, Y. Funahashi, T. Yamaguchi, Y. Fujishiro and M. Awano, "Performance of the Micro-SOFC Module Using Submillimeter Tubular Cells," *Journal of The Electrochemical Society,* vol. 156, no. 3, pp. B318-B321, 2009.

P. Sarkar, L. Yamarte, H. Rho and L. Johanson, "Anode-Supported Tubular Micro-

18] Solid Oxide Fuel Cell," *Int. J. Appl. Ceram. Technol.*, vol. 4, no. 2, pp. 103-108, 2007.

A. Bieberle-Hutter and e. al., "A micro-solid oxide fuel cell system as battery
19] replacement," *Journal of Power Sources,* vol. 177, pp. 123-130, 2008.

Z. Shao and S. M. Haile, "A high-performance cathode for the next generation of
20] solid-oxide fuel cells," *Letters to Nature,* vol. 431, pp. 170-173, 2004.

S. Rey-Mermet and P. Muralt, "Materials and Design Study for Micromachined
21] Solid Oxide Fuel Cells Membranes," *Mater. Res. Soc. Symp. Proc.,* vol. 972, 2007.

T. Talebi, M. Haji and B. Raissi, "Effect of sintering temperature on the
22] microstructure, roughness and electrochemical impedance of electrophoretically deposited YSZ electrolyte for SOFCs," *International Journal of Hydrogen Energy,* vol. 35, pp. 9420-9426, 2010.

S. T. Aruna and K. S. Rajam, "A study on the elctrophoretic deposition of 8YSZ
23] coating using mixture of acetone and ethanol solvents," *Materials Chemistry and Physics,* vol. 111, pp. 131-136, 2008.

F. Chen and M. Liu, "Preparation of yttria-stabilized zirconia (YSZ) films on
24] La0.85Sr0.15MnO3 (LSM) and LSM-YSZ substrates using an electrophoretic deposition (EPD) process," *Journal of the European Ceramic Society,* vol. 21, pp. 127-134, 2001.

P. Sarkar and P. S. Nicholson, "Electrophoretic Deposition (EPD): Mechanisms,
25] Kinetics, and Applications to Ceramics," *J. Am. Ceram. Soc. ,* vol. 79, no. 8, pp. 1987-2002, 1996.

T. Ishihara, K. Sato and Y. Takita, "Electrophoretic Deposition of Y2O3-stabilized
26] ZrO2 electrolyte films in Solid Oxide Fuel Cells," *J. Am. Ceram. Soc.,* vol. 79, no. 4, pp. 913-919, 1996.

I. Zhitomirsky and A. Petric, "Electrophoretic deposition of electrolyte materials for
27] solid oxide fuel cells," *Journal of Materials Science,* vol. 39, pp. 825-831, 2004.

I. Zhitomirsky and A. Petric, "Electrolytic deposition of zirconia and zirconia
28] organoceramic composites," *Materials Letters,* vol. 46, pp. 1-6, 2000.

L. Besra, S. Zha and M. Liu, "Preparation of NiO-YSZ/YSZ bi-layers for solid oxide
29] fuel cells by electrophoretic deposition," *Journal of Power Sources,* vol. 160, pp. 207-214, 2006.

H. Tomaszewski, J. Haemers, N. De Roo, J. Denul and R. De Gryse, "Yttria-
30] stabilized zirconia thin films grown by r.f. magnetron sputtering from an oxide target," *Thin Solid Films,* vol. 293, pp. 67-74, 1997.

H. Tomaszewski, J. Haemers, J. Denul, N. De Roo and R. De Gryse, "Yttria-
31] stabilized zirconia thin films grown by reactive r.f. magnetron sputtering," *Thin Solid films,* vol. 287, pp. 104-109, 1996.

M. Tsuchiya, B.-K. Lai and S. Ramanathan, "Scalable nanostructured membranes
32] for solid-oxide fuel cells," *Nature Nanotechnology,* vol. 6, pp. 282-286, 2011.

J. Wu, S. Kim, W. Chen, A. Carlson, K.-C. Hwang, Y. Huang and J. A. Rogers,
33] "Mechanics of reversible adhesion," *Soft Matter,* vol. 7, pp. 8657-8662, 2011.

C.-C. Chao, C.-M. Hsu, Y. Cui and F. B. Prinz, "Improved Solid Oxide Fuel Cell
34] Performance with Nanostructured Electrolytes," *ACS Nano,* vol. 5, no. 7, pp. 5692-5696, 2011.

T. Suzuki, Z. Hasan, Y. Funahashi, T. Yamaguchi, Y. Fujishiro and M. Awano,
35] "Impact of Anode Microstructure on Solid Oxide Fuel Cells," *Science,* vol. 325, pp. 852-855, 2009.

T. Suzuki , H. Zahir, T. Yamaguchi, Y. Fujishiro, M. Awano and N. Sammes,
36] "Fabrication of micro-tubular solid oxide fuel cells with a single-grain-thick yttria stabilized zirconia electrolyte," *Journal of Power Sources,* vol. 195, no. 23, pp. 7825-7828, 2010.

J. H. Joo and G. M. Choi, "Simple fabrication of micro-solid oxide fuel cell

37] supported on metal substrateq," *Journal of Power Sources,* vol. 182, pp. 589-593, 2008.

S. Rey-Mermet and P. Muralt, "Solid oxide fuel cell membranes supported by nickel
38] grid anode," *Solid State Ionics,* vol. 179, pp. 1497-1500, 2008.

P. Brown, T. Khan, Y. A. Vlasov, P. Batista, F. Leon, D. Dixon, G. L. Larkins, P.
39] Stampe and R. J. Kennedy, "YBa2Cu3O7 on Sputter Deposited YSZ Buffered Si (100)," *Physica C,* Vols. 341-348, pp. 2407-2408, 2000.

G. J. La O, J. Hertz, H. Tuller and Y. Shao-Horn, "Microstructrual Features of RF-
40] sputtered SOFC Anode and Electrolyte materials," *J. of Electroceramics,* vol. 13, pp. 691-695, 2004.

A. Nagata and H. Okayama, "Characterization of solid oxide fuel cell device having
41] a three-layer film structure grown by RF magnetron sputtering," *Vacuum,* vol. 66, pp. 523-529, 2002.

N. Nakagawa, H. Yoshioka, C. Kuroda and M. Ishida, "Electrode performance of a
42] thin-film YSZ cell set on a porous ceramic substrate by rf sputtering technique," *Solid State Ionics,* vol. 35, pp. 249-255, 1989.

F. Smeacetto, M. Salvo, L. C. Ajitodoss, S. Perero, T. Moskalewicz, S. Boldrini, L.
43] Doubova and M. Ferraris, "Yttria-stabilized zirconia thin film electrolyte produced by RF sputtering for solid oxide fuel cell applications," *Materials Letters,* vol. 64, pp. 2450-2453, 2010.